Korean J. Chem. Eng., 39(3), 529-547 (2022)
DOI: 10.1007/s11814-021-0907-0

pISSN: 0256-1115
eISSN: 1975-7220

Sorption thermodynamics and coupling effect for pervaporative dehydration of acetone through nanoclay and iron nanoparticle-filled copolymer membranes

Swastika Choudhury and Samit Kumar Ray†

Department of Polymer Science and Technology, University of Calcutta, 92, A. P. C. Road, Kolkata-700009
(*Received 5 May 2021 • Revised 6 July 2021 • Accepted 13 July 2021*)

Abstract−Sodium montmorillonite (NaMMT) nanoclay particles were incorporated *in-situ* in the copolymer matrix of Poly (acrylonitrile-co-ethyl acrylate) during its synthesis from different molar% of acrylonitrile (AN) and ethyl acrylate (EA) monomers by emulsion polymerization. Similar polymerization was also carried out in the presence of iron salts to generate iron nanoparticles (FeNP) *in situ* in the membrane matrix. The membranes were characterized by FTIR, NMR, molecular weight (M_v), XRD, DTA-TGA, SEM, TEM, EDAX, contact angles for hydrophilicity and mechanical properties. The sorption and permeation of acetone-water binary mixtures through these membranes were analyzed in terms of solvent-solvent and solvent-membranes interaction and also by solvent coupling with Flory-Huggins, ENSIC and six-parameter solution diffusion model. The synthesis variables were optimized with the central composite design (CCD) of response surface methodology (RSM). The filled membranes showed high sorption and pervaporation selectivity for water for dehydration of acetone, while for similar filler loading FeNP-filled membranes showed higher flux and selectivity than NaMMT clay filled membrane. The membrane prepared with AN : EA molar ratio of 5 : 1 and filled with 2 wt% NaMMT clay showed a flux(kg/m^{2}h)/selectivity of 0.903/125.2, which further increased to 0.937/140 for the same membrane filled with 5 wt% FeNP for 90 wt% feed acetone.

Keywords: Poly (AN-co-EA), NaMMT Clay, FeNP, Acetone-water Mixture, Sorption Thermodynamics, Pervaporation and Flow Coupling

INTRODUCTION

Two separate polymers having different properties may be combined in a polymer blend or in a copolymer. A copolymer is chemically more stable than a polymer blend because of covalent carbon bonding of the two different repeating units of the constituent monomers. The monomers are chosen in such a way that the repeating units of one monomer provide mechanical and chemical stability, while the repeating units of the other monomer contribute to permeability and selectivity for one of the permeants. Thus, no crosslinker is required for preparing a copolymer membrane since one of the repeating units provides solvent resistance without any additional need of a crosslinker. Further, there are many functional homopolymers which cannot form mechanically and chemically stable polymer film or membranes. The monomers of these functional polymers may be grafted to a stable film forming polymer or copolymerized with monomers of these film forming polymers. Polyethyl acrylate is a soft elastomeric polymer with a very low (–23 °C) glass transition temperature [1]. However, mechanically stable film forming polymer may be synthesized from its copolymers with ethylene [2], methyl methacrylate [3], styrene [4] and acrylonitrile [5].

The different copolymers of polyacrylonitrile (PAN) have been reported as efficient membrane materials for enzyme immobilization, dialysis, ultrafiltration and pervaporation applications [6]. The copolymers of acrylonitrile with acrylic acid [7], hydroxyethyl methacrylate (HEMA) [8], itaconic acid [9], maleic anhydride [10], N-vinylpyrrolidone [11] and butyl acrylate [12], were reported as hydrophilic membranes. Similarly, the copolymers of styrene with butyl acrylate [13], methyl methacrylate [14] and vinyl acetate [14] were reported as organophilic membranes for applications in pervaporation (PV). To further improve its permeability, micro and nano sized inorganic fillers were also incorporated into polyacrylonitrile (PAN) copolymers [7,11-13]. However, the limitation of the compatibility between inorganic clay and organic polymer affects the selectivity of the membranes. The poor compatibility of inorganic clay materials is evident from its agglomeration in the polymer matrix, which is observed in its scanning electron micrographs (SEMs).

Inorganic clay materials of micron size dimension may be incorporated into a polymer matrix with higher loading% than the nanosized clay. However, the nanosized clay has much higher specific surface area and surface energy than the micron size clay. Small amounts of nano materials significantly improve the mechanical stability and permeability of the filled membranes [8,15-27]. Thus, graphene nanoparticles loaded sodium alginate [16] and chitosan [17] composite membranes showed high water selectivity for pervaporative dehydration of 10 wt% isopropyl alcohol [16,17] and ethanol [17]. Treatment of graphene with hydrogen peroxide further improved selectivity of chitosan-polyvinyl pyrrolidone blend membranes [18]. The down side of nanomaterials is poor stability, easy agglomeration even at lower loading% in the polymer matrix and high cost. The high cost and susceptibility of nanomaterials to agglomeration in the polymer matrix may be countered by generating

†To whom correspondence should be addressed.
E-mail: samitcu2@yahoo.co.in
Copyright by The Korean Institute of Chemical Engineers.

nanometal or nanometal oxides *in situ* from low cost bulk metal salts either in the presence of the polymer solution or during synthesis of the polymer from its monomers. Accordingly, silver nanoparticles (AgNPs) were generated *in situ* by reduction of silver salts in aqueous solution of PVA [19,20] and PVA-polyacrylic acid blend [21]. The resulting AgNPs filled membranes showed much higher flux and selectivity than the unfilled membranes. Similar to AgNPs, iron nanoparticles (FeNPs) were also generated in PAN-HEMA-grafted PVA [9], polysulfone [22], PVA [23,24], chitosan [25] and blend of sodium alginate-PAA [26]. The FeNPs were generated either by heating iron carbonyl ($Fe(CO)_5$) in the membrane casting solution [22] or by co-precipitation reaction of ferrous and ferric salts followed by alkali treatment [8,23-25]. These FeNPs filled membranes showed a good balance of flux and selectivity for dehydration of acetone [8,25], acetonitrile [23], IPA, tetrahydrofuran, dioxane [24] and ethanol [26,27]. Accordingly, in the present work several copolymers (CP) of AN and EA were prepared and during polymerization FeNPs were generated *in situ* by co-precipitation of Fe^{+2} ($FeSO_4$, $7H_2O$) and Fe^{+3} ($FeCl_3$, $6H_2O$) salts at different molar ratios in the matrix of the CP. Similarly, NaMMT nanoparticles were also incorporated into the growing CP matrix. The unfilled and filled copolymer membranes were characterized and used for analysis of sorption and pervaporation of acetone-water mixtures. As a solvent, acetone was chosen since this volatile solvent is industrially very significant with widespread use of aqueous acetone in paint, plastics, leather, explosive and pharmaceutical industries [28]. Further, acetone-water mixture is also generated during its production from IPA by catalytic oxidation [29]. However, separation of low concentration of water from acetone by distillation is expensive because of the requirement of high reflux and large column. A hybrid distillation-pervaporation process consisting of distillation of acetone-water mixtures to a mixture of low water concentration (<10 wt%) followed by a final pervaporative dehydration would be very attractive and energy efficient [29]. The dehydration of acetone by pervaporation has also been reported by many researchers [29-33]. The novelty of the present work lies in i) incorporation of *in-situ* generated iron nanoparticles into a growing copolymer matrix instead of its incorporation into a homopolymer or polymer blend solution as reported elsewhere [15-27], ii) synthesis, characterization and use of the copolymer of acrylonitrile (AN) and ethyl acrylate (EA) for the first time as pervaporation membrane and comparison of the effect of iron and clay nanoparticles on separation performance of this copolymer membrane, iii) systematic optimization of synthesis variables with central composite design (CCD) of response surface methodology (RSM) and iv) analysis of sorption and pervaporation in terms of sorption thermodynamics and six-parameter solution diffusion model for these unfilled and filled membranes.

EXPERIMENTAL

1. Materials

High purity analytical grade acetone, acrylonitrile (AN) and ethyl acrylate (EA) monomers (both laboratory reagent grade), potassium persulfate (initiator), sodium lauryl sulfonate (surfactant), ferrous sulfate and ferric chloride were purchased from E. Merck (India) Ltd, Mumbai. The nanosized sodium montmorillonite (NaMMT, polymer grade containing 98% montmorillonite, particle size 30-90 nm, aspect ratio 300-500, mineral's thickness 1 nm, cation exchange capacity 120 meq/100 g) clay was kindly gifted by Amrfeo Pte. Ltd., Kolkata. This nanosized clay was used after drying in a hot oven at 110 °C for 2 h. The monomer acrylonitrile (AN) was extracted with 5 wt% aqueous NaOH solution to remove the inhibitor followed by repeated washing with distilled water till it showed neutral pH before use in polymerization. The other chemicals were used as obtained. Double distilled water prepared in the laboratory was used to make acetone-water feed mixtures.

2. Methods

2-1. Synthesis of Unfilled and Filled CP

2-1-1. Unfilled and NaMMT Clay Particle Filled CP

The copolymer (CP) with AN : EA molar ratios of 3 : 1, 5 : 1, 10 : 1, 15 : 1 and 20 : 1 was prepared by free radical emulsion polymerization of the weighed amounts (total ~15 g monomers in 50 mL water) of monomers in water at 70 °C for around 3 h using potassium persulfate initiator (1 wt% of total monomer weight) in a 100 mL three neck glass reactor fitted with a mechanical stirrer at the central neck, a thermometer and a dropping funnel at the two side necks. During polymerization the weighed amounts (1, 1.5, 2 and 3 wt% of total monomer weight) of NaMMT clay were dispersed in the reaction mixture for its *in-situ* incorporation in the growing CP matrix. The CP prepared with 3 : 1, 5 : 1, 10 : 1, 15 : 1 and 20 : 1 molar ratios of AN : EA were noted as CP3, CP5, CP10, CP15 and CP20, respectively, while the clay-filled polymer containing 1, 1.5, 2 and 3 wt% clay was noted as Clay1, Clay1.5, Clay2 and Clay3, respectively.

2-1-2. Iron Nanoparticle Filled Polymer (FeNP)

FeNP filled copolymer containing 2.5, 5, 7.5 and 10 wt% (of copolymer wt.) FeNPs particles were prepared *in-situ* by co-precipitation of hydrated ferrous and ferric salts in a similar way as reported elsewhere [23-25]. For this synthesis known amount of $FeSO_4 \cdot 7H_2O$ and $FeCl_3 \cdot 6H_2O$ with 1 : 2 molar ratio was added to the copolymerization reaction mixture containing different molar ratios of AN : EA and after adequate stirring the polymerization was allowed in a similar way as for NaMMT-filled polymer. The resulting filled polymers containing 2.5, 5, 7.5 and 10 wt% FeNPs were noted as FeNP2.5, FeNP5, FeNP7.5 and FeNP10, respectively.

2-2. Casting of Membranes

2-2-1. Unfilled and NaMMT Filled Polymer Membranes

The NaMMT-filled and also the unfilled dry polymer were dissolved in DMF (5% w/v) with mechanical stirring till a clear viscous solution was obtained. It was then cast on a clean and smooth glass plate and dried for 24 h at ambient temperature followed by drying in a vacuum oven to remove the traces of the solvents. The dried membranes were peeled off from the glass plates by immersing in water. Finally, the membranes were annealed at 80 °C for an additional 3 h [11].

2-2-2. FeNP Particle Filled Polymer Membranes

The FeNP-particle filled membranes were also prepared by a similar method, except in this case the membrane after drying for 24 h at ambient temperature was immersed in 4 M KOH solution in water for 24 h to generate FeNP particles [25]. The membrane was then repeatedly washed with distilled water until pH neutral-

ity was obtained. It was then dried and used for further study. The thickness of the unfilled and filled copolymer membranes was maintained at around 50 mm and 80 mm, respectively. The thickness was measured by Test method ASTM D 374 using a standard dead weight thickness gauge (Baker, Type J17).

2-3. Membrane Characterization

The various functional groups present in the membrane polymers were characterized by Fourier transform infrared spectroscopy (FTIR). Instead of KBr pallet, the membrane sample was directly taken into the FTIR spectrometer (Perkin Elmer, spectrum-2) for this analysis. The chemical structure of the polymer was analyzed by ^{13}C nuclear magnetic resonance (NMR) on a JEOL, ECX400, 400 MHz NMR spectrometer. The viscosity average molecular weight (M_v) of the membrane polymer was measured from intrinsic viscosity of dilute polymer solutions (0.0020, 0.0030, 0.0040, 0.0050 and 0.0060 g/L in DMF) in an Ubbelohde viscometer. The crystallinity of the membrane samples was determined by wide angle X-ray diffraction (XRD) in a diffractometer (model: X'Pert PRO, made by PANalytical B.V., The Netherlands) with Ni-filtered Cu K_α radiation (λ=1.542 Å) at a scanning rate of 0.005 deg (2θ/s). The thermal characteristics of the polymer samples were characterized by differential thermal analysis (DTA) and thermogravimetric analysis (TGA) in a Mettler instrument in nitrogen atmosphere at the scanning rate of 10 °C/min in the temperature range of 25 to 600 °C. The membrane morphology was characterized by scanning electron microscopy (SEM, S3400N, VP SEM, Type-II, made by Hitachi, Japan) at the accelerating voltage of 15 kV. The membrane polymer samples were also characterized by transfer electron microscopy (TEM, JEM-2100, USA). For TEM analysis a drop of diluted sample specimen was placed on a carbon coated Cu grid on the instrument at 200 kV. Energy dispersive X-ray analyzer (EDAX) coupled with TEM was also used to characterize the elemental composition of the membrane samples. The hydrophilicity of the membranes was evaluated by contact angle measurement using sessile droplet method. The angle made by the water droplet on the membrane surface was measured by a contact angle analyzer (Kruss, DSA 100). The average of three successive readings for each membrane was noted. The mechanical properties, i.e., tensile strength (TS) and elongation at fracture (EAF), were determined in accordance with the ASTM D 882-97 in a universal testing machine of Lloyd (UTM, Lloyd instruments, England).

2-4. Sorption and Permeation by Pervaporation (PV)

2-4-1. Sorption

The sorption or swelling experiments were carried out at 30 °C by immersing around 0.1 g of a thick membrane sample in a stoppered conical flask containing acetone-water binary solvent mixtures of varying concentrations for 96 h to ensure sorption equili-= brium. The solvent swollen sample after being taked out from the flask was carefully blotted between tissue papers to remove the adhered surface solvents. The solvent mixture sorbed in the membrane was removed by a vacuum pump and condensed in a cold trap immersed in liquid nitrogen. The sorbed liquid was analyzed by gas chromatography (GC, Shimadzu, Japan, Column Stabilwax-DAGC, EB624) to measure the concentration of the solvent 1 (i or j) in the membrane (C_{m1}). The total sorption or degree of swelling at equilibrium (Q) is obtained from the difference of wt. of the swollen (W_s) and dry membrane sample (W_d) as

$$Q=\frac{W_s-W_d}{W_d} \tag{1}$$

Similarly, the membrane phase volume fraction of solvents in the solvent-i (water)/solvent-j (acetone)/membrane ternary system is obtained as

$$\phi_{im}=\frac{QC_{im}}{\rho_i}\left(\frac{QC_{im}}{\rho_i}+\frac{QC_{jm}}{\rho_j}+\frac{1}{\rho_p}\right)^{-1} \tag{2a}$$

$$\phi_{jm}=\frac{QC_j}{\rho_j}\left(\frac{QC_{im}}{\rho_i}+\frac{QC_{jm}}{\rho_j}+\frac{1}{\rho_p}\right)^{-1} \tag{2b}$$

where C_{1m} is the wt. fraction of solvent 1 (i or j) in the membrane, ρ_1 is the density of solvent 1, ρ_p is the density of membrane polymer and

$$\phi_{im}+\phi_{jm}+\phi_p=1 \tag{2c}$$

The sorption selectivity for i (water) is obtained as $\alpha_{sorp}=\frac{\phi_{im}/\phi_{jm}}{x_i/x_j}$ (3)

where x_1 is molar fraction of solvent 1 in feed.

2-4-2. Pervaporation

The pervaporation experiments were carried out in a batch stirred cell. The feed volume was 150 cm^3 and the effective membrane area in contact with the membrane cell was 19.6 cm^2. The vacuum (~0.6 kPa) was maintained on the downstream side by a vacuum pump. After filling with acetone-water solvent mixtures, it was equilibrated for 3 h for the first experiment, while 1 h equilibrium time was given for subsequent pervaporation experiments with different feed concentration of acetone. The permeate was collected in a cold trap immersed in liquid nitrogen. The composition of feed and permeate were analyzed by the same GC used for sorption experiment. The results of the pervaporation experiments were reproducible and the inherent error in the measurements was less than 1%.

2-4-3. Molar Flux, Selectivity, Permeability and Membrane Selectivity

The molar flux (kmol/m^2h) of the solvent 1 (i or j) of W g in permeate for Δt time of pervaporation through an effective membrane area of A is obtained as

$$J_{1M}=\frac{W}{M_1\,A\,\Delta t} \tag{4}$$

where M_1 is molecular weight of solvent 1

Pervaporation selectivity for solvent i in a i+j binary mixture is obtained as

$$\alpha_{PV}=\frac{\frac{y_{ip}}{y_{jp}}}{\frac{x_i}{x_j}} \tag{5}$$

Here y_{1p} and x_i are permeate and feed side concentration (wt%) , respectively, of solvent 1. The permeability of solvent 1 (P_1) and intrinsic membrane selectivity (α_{mem}) is defined as [34]:

$$P_1=\frac{J_1L}{(x_{f1}\gamma_{f1}p_{f1}^{sat}-y_{p1}p_p)}=\frac{J_1L}{(f_1-y_{p1}p_p)} \tag{6a}$$

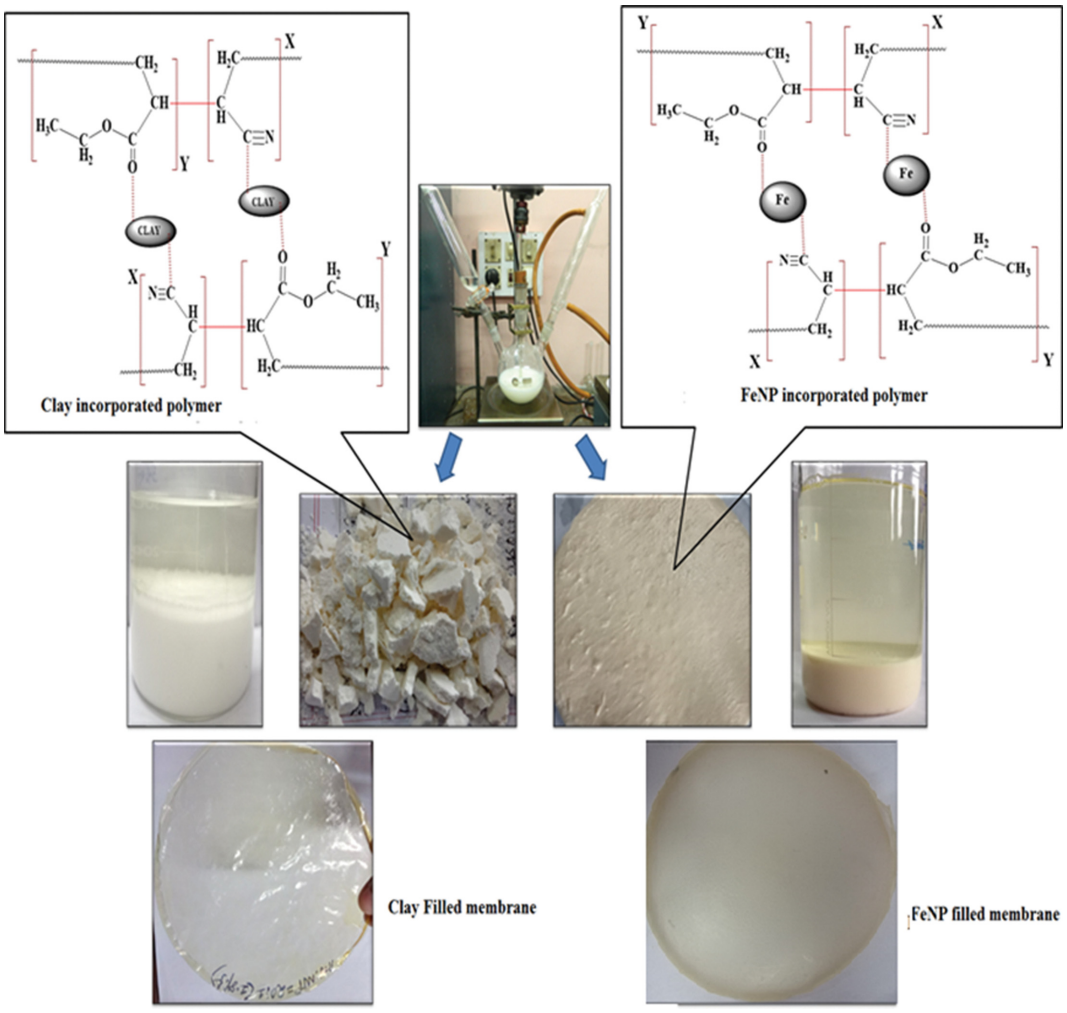
$$\alpha_{mem} = \frac{P_i}{P_j} \quad (6b)$$

where f_1, x_1, and y_{1p} are feed side fugacity, feed side molar fraction and permeate side molar fraction of solvent 1 (i or j), respectively, γ_{f1} is feed side activity coefficient of solvent 1 determined from feed concentration by Wilson parameter (Λ_{ij}=0.7407, Λ_{ji}=0.06448) [35], p_{f1}^{sat} is saturated vapor pressure of solvent 1 on feed side obtained by Antoine equation and P_p is the total pressure on the permeate side of the membrane.

RESULTS AND DISCUSSION

1. Synthesis of the Nanoparticle-filled Copolymer

The objective of the present work was to prepare a strong hydrophilic membrane which should also tolerate highly concentrated (80-99 wt%) acetone in feed. Polyacrylonitrile is a stable polymer, which is not chemically attacked by concentrated acetone but it has limited affinity for water. Thus, in the present work acrylonitrile was copolymerized with ethyl acrylate where the acrylate functionality is likely to attract more water molecules. Thus, depending on the relative reactivity ratios, five different copolymers of AN and EA were prepared with AN : EA molar ration of 3 : 1, 5 : 1, 10 : 1, 15 : 1 and 20 : 1. The polymer prepared from AN : EA molar ratio below 3 : 1 became soft and rubbery because of the presence of excess EA rubbery unit in the copolymer. Hence, membrane of acceptable mechanical stability could not be cast from copolymer with molar ratio of AN : EA<3. Similarly, for AN : EA molar ratio >20 : 1, because of excess nitrile moiety, the membrane became fibrous with very low water absorption. Thus, molar ratio of AN : EA was kept in the range of 3 : 1 to 20 : 1. Among the different polymerization techniques, free radical emulsion polymerization in water is very simple and it leads to a high molecular weight polymer from which a mechanically stable polymer membrane can be prepared. Thus, in the present work emulsion polymerization was employed. For better polymer-clay compatibility, the NaMMT clay was incorporated *in- situ* into the polymer matrix instead of conventional physical mixing of the unfilled polymer with the clay particles. In fact, nanoparticles like NaMMT tend to agglomerate during physical mixing while *in situ* gradual incorporation of the nanoclay into the matrix of the growing copolymer during polymerization gives much better polymer-clay compatibility [7]. The



Scheme 1. Clay-filled and FeNP-filled membrane and its probable statucture.

NaMMT clay enhanced the mechanical stability and hydrophilicity of the filled membranes.

1-1. FeNPs

Similarly, iron oxide nanoparticles (FeNPs) were incorporated in the copolymer matrix by co-precipitation in the polymerization mixture. Ferromagnetic nanosized iron oxide particles exist as Fe_3O_4 and γ-Fe_2O_3. In *in-situ* method the generation of both low and high concentration (0-60%) of iron nanoparticles (FeNPs) is possible in polymer matrix after the percolation threshold [43]. The iron ions immobilized in the copolymer by numerous nitrile (-CN) and ester (CO_2Et) functionalities of the copolymer and also the OH- groups of KOH resulting in the formation of FeNPs as black Fe_3O_4 or brown colored γ-Fe_2O_3 depending on the molar ratio of ferrous and ferric salt used in the reaction. A 1 : 1 molar ratio of these salts leads to the formation of FeNPs with dominance of black Fe_3O_4 while the 1 : 2 molar ratio leads to the dominance of brown colored γ-Fe_2O_3 [23-25]. Accordingly, in the present work the nanoparticle formation was also physically manifested by gradual changing of the initially transparent copolymer membrane to yellow brown color (Scheme 1) due to the dominance of γ-Fe_2O_3 in the membrane. Below 1% clay or 2.5% FeNP, the improvement in flux and selectivity of the filled membranes was marginal, while above 3/7.5% of Clay/FeNP, the membrane-filler compatibility became poor. Thus, Clay/FeNP was fixed in the range of 1/2.5%

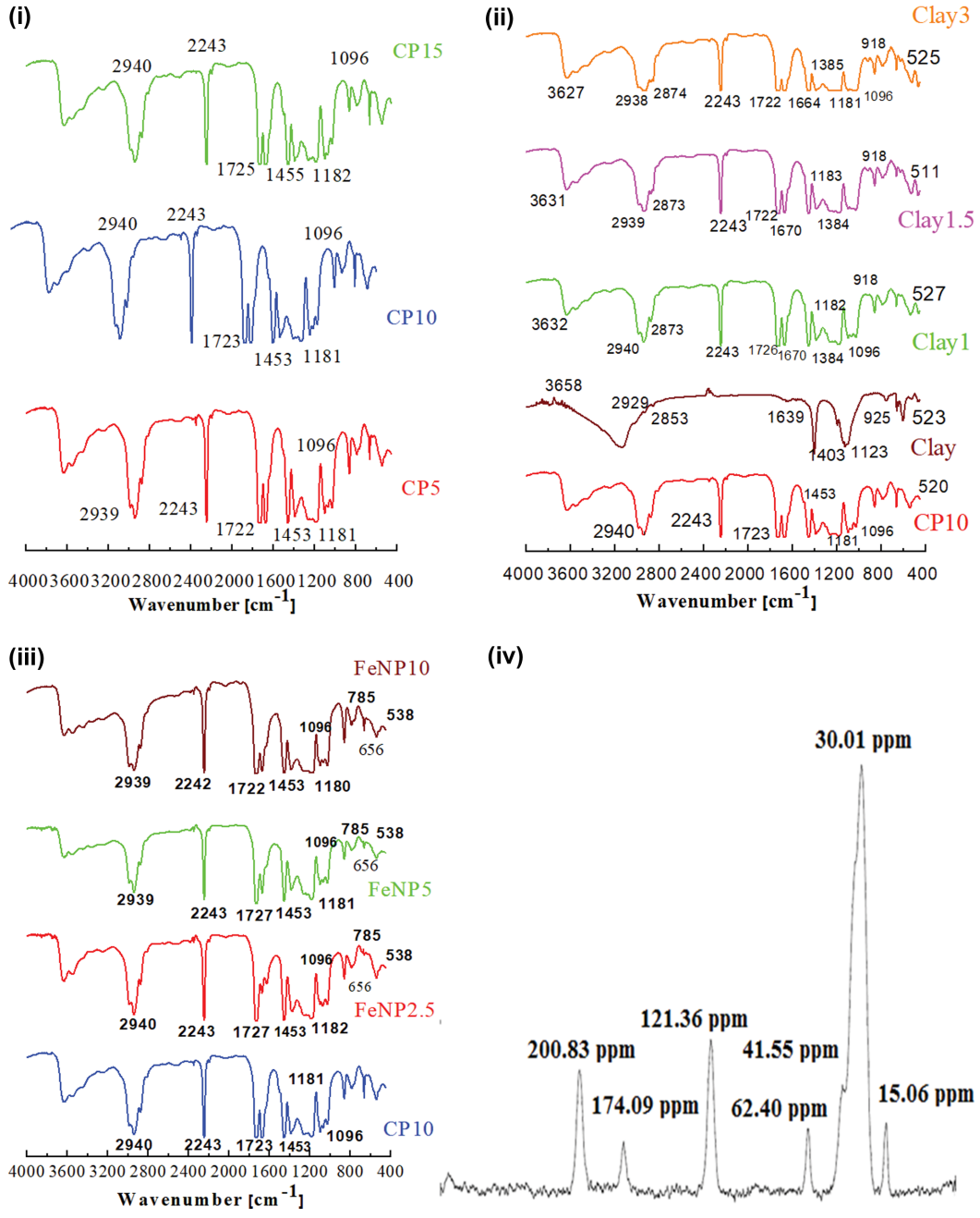


Fig. 1. (i) FTIR of unfilled copolymer, (ii) clay and clay-filled copolymer, (iii) FeNP-filled copolymer, (iv) NMR of the unfilled copolymer (CP5).

to 3/7.5%. The clay-filled and FeNP-filled membrane prepared by these methods and its probable structure is shown in Scheme 1.

2. Characterization of the Membranes

2-1. FTIR

The FTIR of the CP5, CP10 and CP15 copolymers prepared with 5 : 1, 10 : 1 and 15 : 1 of AN : EA molar ratios, respectively, is presented in Fig. 1(i). In the absence of standard sample of known copolymer composition, it is not possible to find the quantitative copolymer composition of an unknown sample. However, the different copolymer compositions may be qualitatively determined from the relative values of the ratio of the characteristic peaks (to eliminate the thickness variation of two samples) of the comonomer moiety [7]. The characteristic nitrile (CN) peak of the AN moiety and carbonyl (CO) peak of the ethyl acrylate moiety is observed at 2,243 cm^{-1} and at 1,722 cm^{-1}, respectively, with varied intensities. The values of peak ratios due to absorption at 2,243 cm^{-1}/1,722 cm^{-1} increased from CP5 to CP15 indicating increase in the amount of AN in the membrane in the same order. In Fig. 1(ii) some of the characteristic absorption peaks of NaMMT clay are also observed in the clay filled Clay1, Clay1.5 and Clay3 polymer. Accordingly, the absorption peaks of NaMMT clay at 3,658 cm^{-1} due to O-H stretching of its silanol (Si-OH) group, 523 cm^{-1} due to Si-O-Si groups of its tetrahedral sheet and the absorption band at 1,640 cm^{-1} corresponding to bending of H-OH bond of water molecules in the clay matrix [7,11] are shifted to 3,632 cm^{-1}/3,631 cm^{-1}/3,627 cm^{-1}, 527 cm^{-1}/511 cm^{-1}/525 cm^{-1} and 1,670 cm^{-1}/1,670 cm^{-1}/1,664 cm^{-1} in Clay1, Clay1.5 and Clay3, respectively. The FTIR of the iron nanoparticle-filled polymers is shown in Fig. 1(iii). The iron nanoparticle-filled copolymers are observed to show some additional peaks apart from the peaks of the AN and EA moiety. These additional peaks, i.e., the absorption peaks at 538 cm^{-1} and 656 cm^{-1} correspond to the presence of iron nanoparticles in the filled FeNP2.5, FeNP5 and FeNP510 polymers as reported elsewhere [44]. The 100 MHz ^{13}C NMR of the unfilled 10 : 1 poly (AN-co-EA) copolymer (noted as CP10) is shown in Fig. 1(iv). Pure polyacrylonitrile has been reported [45,46] to show three different strong chemical shifts (∂, in ppm) for its C1 (the nitrile, CN functionality), C2 (carbon adjacent to CN) and C3 (-CH_2) carbon at 120.5 ppm, 28.3 ppm and 33.3 ppm, respectively. The C1 or nitrile peak of the copolymer of acrylonitrile with ethyl acrylate is shifted at 121.36 ppm and the C2 peak of acrylonitrile moiety is shifted to 30.01 ppm in the copolymer.

2-2. ^{13}C NMR

^{13}C NMR of pure polyethyl acrylate has been reported [47] to show several peaks: at 14-15 ppm for its methyl carbon (-CH_3), CH main chain at 41.92 ppm, -OCH_2 at 60.95 ppm and carbonyl (C=O) at 174.95 ppm. These chemical shifts of ethyl acrylate are also observed at 15.06 ppm, 41.5 ppm, 62.401 ppm and 174.09 ppm in the copolymer. Similarly, homo polyacrylonitrile (PAN) was reported to show a characteristic chemical shift for its aliphatic carbon at 33 ppm and a strong signal at 121 ppm due to its nitrile (CN) functionality [47,48]. The present copolymer is also observed to show a chemical shift at 121.36 ppm and 30.01 ppm, which may be due to the presence of AN moiety in the copolymer. Thus, the copolymer was successfully prepared as is evident from the presence of characteristic chemical shifts of both acrylonitrile and ethyl acrylate moiety in the copolymer.

2-3. Viscosity Average Molecular Weight (M_v) of the Polymer

The viscosity (η) of different low concentrations (C=0.0020, 0.0030, 0.0040, 0.0050 and 0.0060 g/L in DMF) of the CP5, CP10 and CP15 polymers was obtained in an Ubbelohde viscometer. The intrinsic viscosity ([η]) of these polymers was obtained by extrapolating the linear plot of η versus C to zero concentration (y axis). The viscosity average molecular weight (M_v) of the polymers was obtained from intrinsic viscosity ([η]) by using the following Mark-Houwink equation:

$$[\eta] = KM_v^a \tag{21}$$

The values of Mark-Houwink constant 'K' and 'a' for these copolymers of acrylonitrile (AN) and ethyl acrylate (EA) were obtained from literature [49,50]. Accordingly, the M_v (g/mole) of the three polymers, CP5, CP10 and CP15, were obtained as 0.58×10^5, 1.6×10^5, 1.82×10^5 and 1.98×10^5, respectively. In fact, high molecular weight polymer is obtained by emulsion polymerization as in the present work. The membranes prepared from these polymers or the same polymers filled with clay or iron nanoparticles will be of good mechanical strength because of high M_v and these membranes will be suitable for pervaporative separation. The increase in M_v from CP5 to CP15 may be ascribed to the decrease in molar% of EA in the polymers. The molar volume of EA is higher than AN. Thus, the propagation of the polymer radicals increases with decrease in EA content in the copolymer from CP5 to CP15, resulting in increase in M_v in the same order [50]. Similar order of M_v values were also reported for other AN copolymers [50].

2-4. XRD Analysis

The wide angle XRD of the NaMMT clay, CP, Clay1, Clay1.5, Clay2 and Clay3 filled copolymers is shown in Fig. 2(i). The XRD of the 5 wt% iron oxide nano particle (FeNP) filled copolymer (noted as FeNP5) is shown in Fig. 2(ii). The XRD peak at two theta of 17.2° to 17.5° for a *d* spacing of 5.15 A° as observed in Fig. 2(i) and Fig. 2(ii) is due to polyacrylonitrile as reported elsewhere [51]. Accordingly, the unfilled copolymer (CP10) shows the XRD peak of its polyacrylonitrile moiety at 17.5°. The NaMMT clay shows several peaks at 20.5°, 36°, 54.6°, 62.5° and 73.6° as also reported elsewhere [52]. However, the XRD peaks of NaMMT clay are not observed in the clay filled copolymers, indicating the exfoliation of the clay particles in the polymer matrix [11]. In fact, NaMMT or FeNP nanoparticles are incorporated in the copolymer from the aqueous phase and as the polymer sample is dried by evaporation, the nanoparticles solidifies rapidly in the polymer matrix with limited mobility of its molecules. Hence, the crystalline structure of NaMMT or FeNP is not properly developed in the polymer matrix [53]. The diffused peak at 24.12° as observed for FeNP5 in Fig. 2(ii) corresponds to the iron oxide nanoparticles with 012 lattice plane as reported elsewhere [54].

2-5. DTA-TGA

The DTA and TGA of the NaMMT-clay filled and FeNP-filled copolymer membrane is shown in Fig. 2(iiia) and 2(iiib), respectively. It is observed that in the temperature range of 20-600 °C, both filled copolymers show excellent thermal resistance properties. The initial 2-5% weight loss in the temperature range of 60-100 °C for FeNP-filled copolymer and 100-250 °C for clay filled

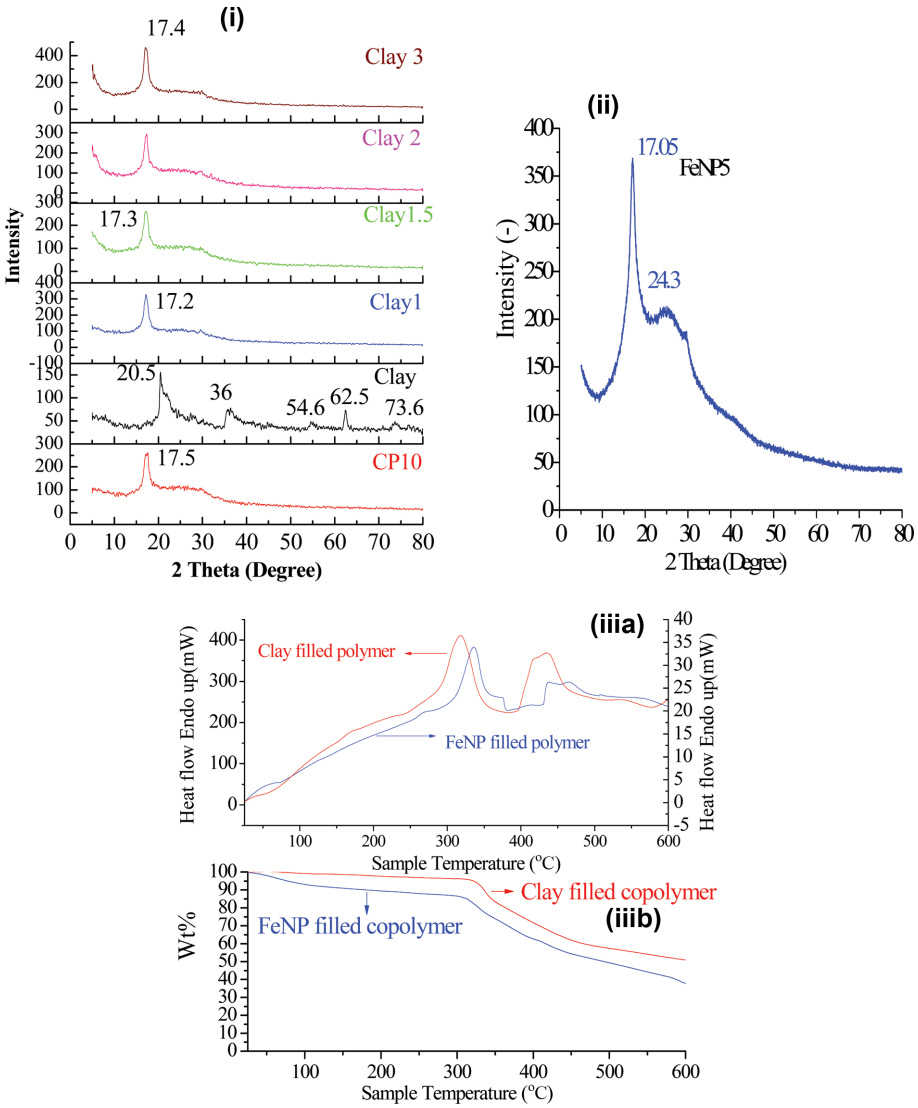


Fig. 2. (i) XRD of copolymer, Clay and Clay filled copolymer, (ii) XRD of FeNP filled copolymer, (iii) DTA-TGA of clay filled and FeNP filled polymer.

polymer is due to the loss of physically adsorbed water. Both polymers show two major degradation profiles-one in the temperature range of 100-300 °C where clay filled polymer shows a weight loss of around 2-5%, while FeNP polymer shows a degradation of 2-14%. From 320-600 °C both polymers degrade at an exponential rate with a degradation of 5-50% for clay-filled polymer and 15-60% for FeNP-filled polymer. This may be due to the splitting of main polymer chain. Consequently, in the DTA curve, the clay-filled polymer shows two endothermic peaks at around 315 and 430 °C, while FeNP-filled polymer shows similar peaks at 315 and 436 °C. From DTA-TGA result it is evident that the membrane prepared from clay- or FeNP-filled polymer will remain thermally stable in the pervaporation experiment, which is usually carried out at low temperature (25-50 °C).

2-6. SEM, TEM and EDAX Analysis

The SEMs of the clay filled Clay1, Clay1.5, Clay2 and Clay3 membranes are shown in Fig. 3(i)-(iv), respectively. The SEMs were carried out at 15 kV and at a high 10,000x magnification. The clay particles were observed to be evenly distributed in the CP polymer matrix. However, with an increase in clay loading polymer-clay compatibility becomes increasingly difficult and agglomeration of these clay particles is evident in Clay3 (Fig. 3(iv)) membrane. The SEMs of the FeNP5 and FeNP10 membranes are shown in Fig. 3(v) and (vi), respectively. Both membranes show a uniform distribution of iron oxide nanoparticles in the copolymer matrix without any agglomeration. The FeNP5 membrane prepared with more diluted iron salt shows marginally smaller iron particles than FeNP10 prepared with higher concentration of salt, which may be due to the slower rate of *in situ* generation of iron nanoparticles in the copolymer matrix. The TEM analysis of FeNP5, presented in Fig. 3(vii) and (viii), shows an average particle size of 50 nm of the iron nanoparticles without any measurable agglomeration, while the TEM-EDAX data presented in Fig. 3(ix) also shows the presence of the elemental iron, carbon and nitrogen in FeNP5 filled copolymer.

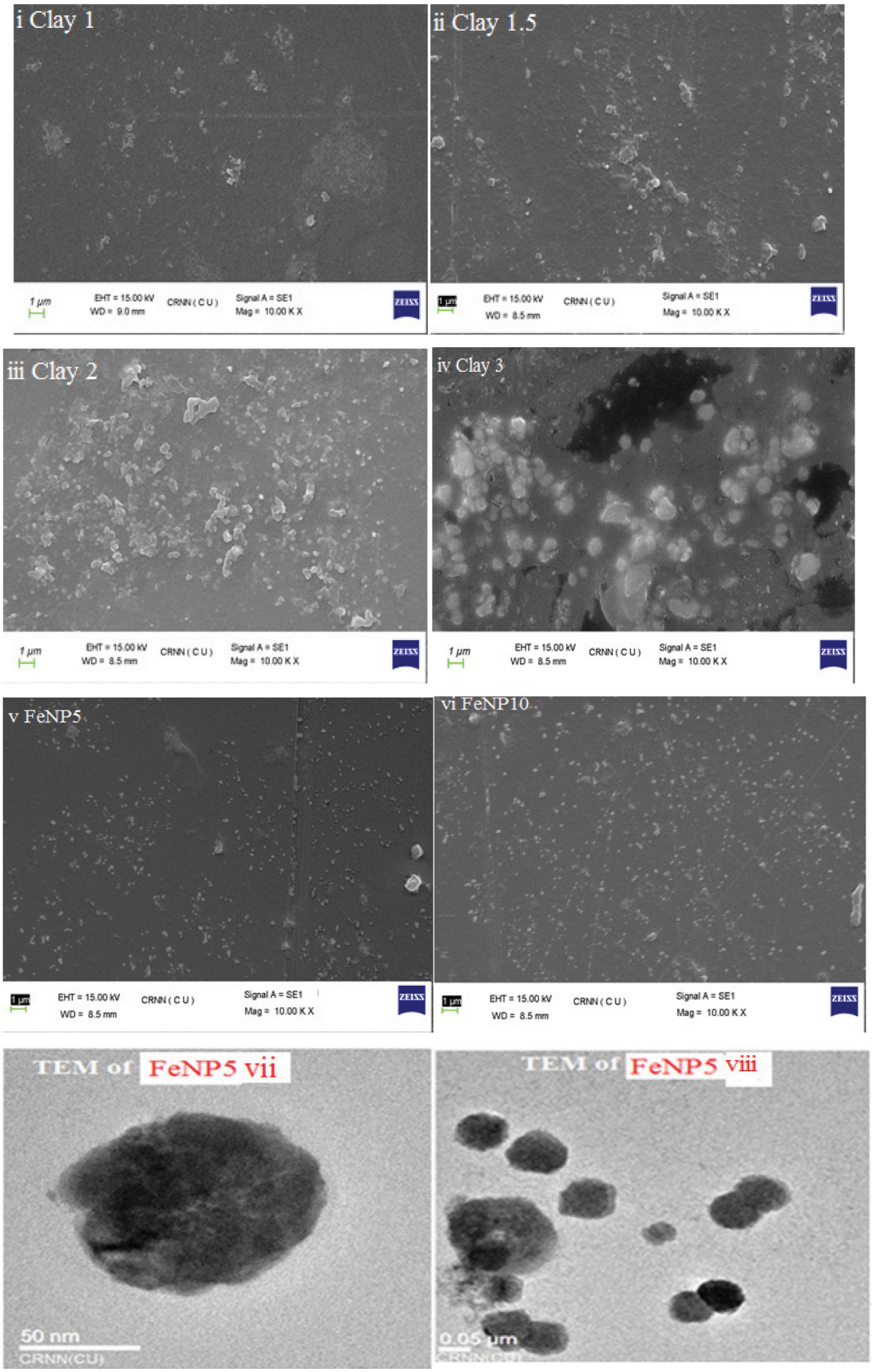


Fig. 3. SEM of (i)-(iv) clay-filled CP, (v)-(vi) FeNP-filled CP, (vii)-(viii) TEM of FeNP5, (ix) TEM-EDAX of FeNP5 and (x) contact angles of the unfilled and filled membranes.

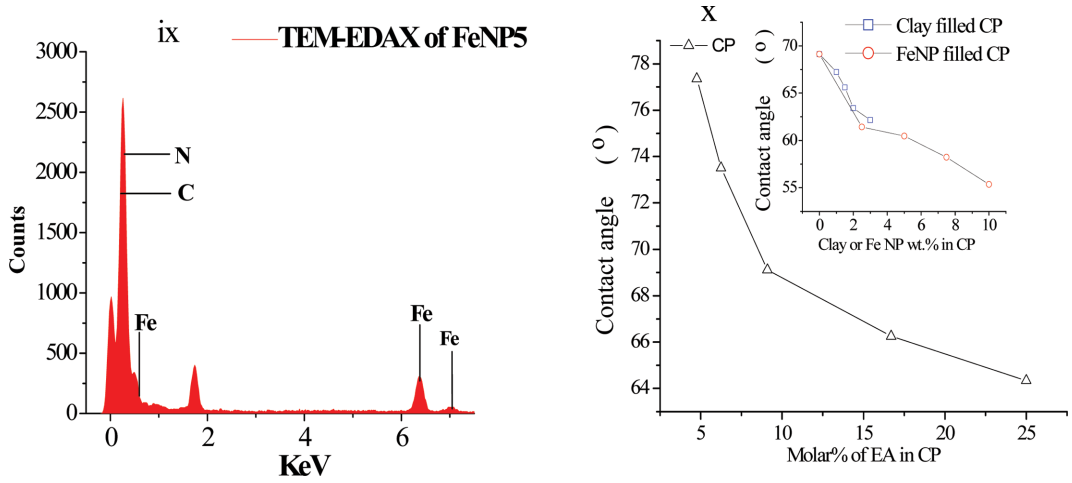


Fig. 3. Continued.

2-7. Contact Angle Properties

The hydrophilicity of the unfilled and nanoparticles filled copolymer membranes was evaluated by contact angle measurement using sessile droplet method. The contact angle should be equal or less than 90° ($\theta \leq 90°$) for a hydrophilic membrane. The lower the contact angle, the higher will be the hydrophilicity of the membrane. The variation of contact angles made by water on the membrane surface for different molar% of ethyl acrylate (EA), wt% of clay and also wt% of iron nanoparticles (FeNP) in the copolymer (CP) is shown in Fig. 3(x). It is observed that with increase in ethyl acrylate (EA) content the contact angle decreases from CP20 containing 4.76 molar% EA to CP3 containing 25 molar% EA. Hence, the hydrophilicity of the unfilled membrane increases in the same order. Addition of nanoparticles causes a decrease in contact angle and increase in hydrophilicity of a hydrophilic membrane [16-18, 25,27]. Similarly, from the inset of Fig. 3(x) it is also observed that the contact angles of the present copolymer membranes decrease in the presence of the nanoclay and iron nanoparticles. Thus, the hydrophilicity of the filled membranes also increases with increase in filler (clay or iron nanoparticles) loading in the membrane.

2-8. Mechanical Properties

The mechanical properties of the different polymers synthesized in the present work and used for preparation of pervaporation membranes are shown in Table 1. The higher the tensile strength (TS), the higher will be the mechanical stability of the membrane. On the other hand, the higher the elongation at fracture (EAF), the higher will be the flexibility of the membrane. Very high TS with low EAF makes a membrane hard and brittle, while very high EAF with low TS makes a membrane too soft. Hence, there should be a good balance between TS and EAF. The present polymers show a good balance of high TS and acceptable EAF as observed in Table 1. As the amount of polyacrylonitrile moiety increases in the copolymer, TS and EAF increase from CP3 to CP20. Polyacrylonitrile, a film and fiber forming polymer, has very high tensile strength (44.81 MPa) and modulus (1,296.3 MPa) as reported elsewhere [55]. In contrast, polyethyl acrylate homopolymer has rubbery properties with low tensile strength and elongation. Thus, with the increase in acrylonitrile content, the mechanical properties, i.e., TS and EAF, of the copolymer membranes increases from CP3 to CP20. Similarly, with increase in clay% from 0% (CP10) to 1% the TS increases from 13.06 MPa to 29.80 MPa, which further increases to 37.92 MPa and 45.98 MPa at a clay loading of 1.5 and 2%, respectively. However, at 3 wt% clay loading clay-polymer compatibility becomes poor because of the agglomeration of clay particles in the polymer matrix (Fig. 3(iv)) and thus TS decreases to 35.12 MPa, which is still higher than TS of the unfilled or filled membrane containing 1 wt% clay. On the other hand, incorporation of clay reduces chain mobility and thus EAF decreases from Clay1 to Clay3. SA similar trend is also obtained with FeNP-filled membrane. From Table 1 it is also evident that the TS and EAF of the unfilled and filled polymers are high enough to make the membranes durable without any failure during sorption and pervaporation experiments.

Table 1. Tensile property of the polymers

Membrane	Tensile strength (MPa)	Elongation at fracture (mm)
CP3	6.56	11.28
CP5	7.82	13.28
CP10	13.06	22.73
CP15	26.08	31.80
CP20	32.82	39.28
Clay1	29.80	27.84
Clay 1.5	37.92	20.84
Clay 2	45.98	18.05
Clay3	35.12	10.903
FeNP10	46.34	12.11
FeNP7. 5	39.51	15.23
FeNP 5	34.22	16.73
FeNP2.5	30.21	18.11

3. Sorption and Permeation Studies

3-1. Sorption

3-1-1. Effect of Copolymer Composition

The effect of copolymer composition on total sorption (Q),

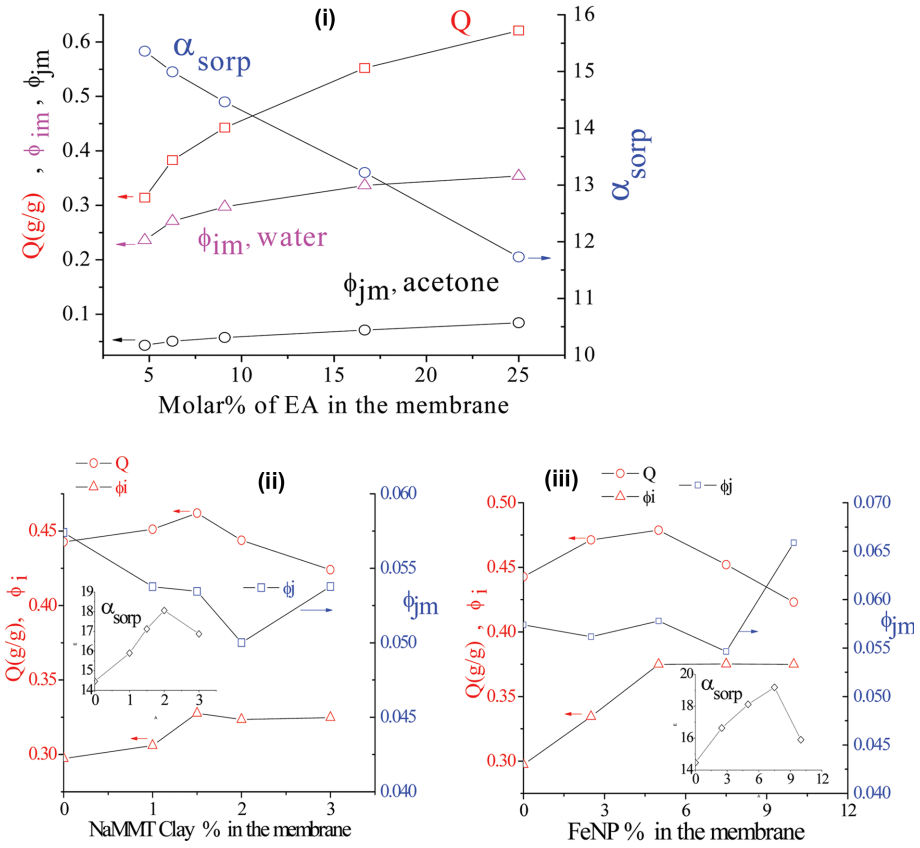


Fig. 4. Effect of (i) copolymer composition, (ii) NaMMT clay wt% in membrane and (iii) FeNP wt% in membrane on total sorption (Q), volume fraction of water (ϕ_i) and acetone (ϕ_j) and sorption selectivity (α_{sorp}).

membrane phase volume fraction of solvent water (ϕ_{im}), acetone (ϕ_{jm}) (refer to 'Theory' given as supplementary document) and sorption selectivity for water (α_{sorp}) is shown in Fig. 4(i). The feed concentration was fixed at 90 wt% acetone in water. It is observed that as the molar% of ethyl acrylate (EA) ester increases in the copolymer, viz, from 4.76% (AN : EA 20 : 1) to 25% (AN : EA 3 : 1), Q, ϕ_{im} and ϕ_{jm} increases . It is also observed that at any copolymer composition, $\phi_{im} >> \phi_{jm}$ while α_{sorp} increases linearly with increase in molar% of AN in the copolymer from 3 : 1 to 20 : 1. In fact, acrylonitrile with its nitrile moiety and ethyl acrylate with its ester moiety contributes to the increased hydrophilicity of the membrane. However, the acrylate ester functionality is more hydrophilic than nitriles. Hence, these trends of sorption results are observed.

3-1-2. NaMMT and FeNPs

From Fig. 4(i) it is evident that at around 10 : 1 molar ratio of AN : EA, the membrane shows optimum Q and α_{sorp}. Thus, the unfilled membrane prepared with 10 : 1 AN : EA molar ratio was further filled with nanosized NaMMT clay and iron nanoparticles (FeNPs). The effect of NaMMT and FeNPs on Q, ϕ_{im}, ϕ_{jm} and α_{sorp} is shown in Fig. 4(ii) and 4(iii), respectively. It is observed that with an increase in wt% of NaMMT clay or FeNPs, initially Q and ϕ_{im} increase up to around 1.5 wt% NaMMT and 5 wt% FeNPs. Above this loading of nanoparticles, both Q and ϕ_{im} decrease. However, the nanoparticle-filled membranes show very low sorption of the organics, i.e., acetone (ϕ_{jm}) and the variation of ϕ_{jm} with filler loadings are also marginal. Similarly, there is a linear increase of α_{sorp} with increase in NaMMT (Fig. 4(ii)) or FeNPs filler (Fig. 4(iii)). In fact, the presence of nanoparticles increases hydrophilicity of the membranes. At the same time the matrix of the membrane becomes denser in the presence of filler. Thus, initially Q and ϕ_{im} increase because of the increased hydrophilicity of the membrane. However, as the filler loading continues to increase, the packing of the membrane matrix becomes very dense. Thus, sorption of the denser membranes decreases. Above 2 wt% NaMMT clay or 7.5 wt% FeNPs there is no further improvement in Q, ϕ_{im} or α_{sorp}. In fact, the attempt of adding NaMMT clay>3 wt% or FeNPs>10% failed during synthesis of the copolymer from its monomer with settling down of filler particles in the bottom of the reactor. From the results of sorption it may be concluded that above 2 wt% clay or 10 wt% FeNPs, the compatibility between inorganic clay or iron nanoparticles and organic polymers becomes poor due to agglomeration, resulting in defect in the morphology of the membrane and subsequent decrease in sorption or sorption selectivity. The SEM analysis also shows agglomeration of the clay particles in the copolymer matrix at 3 wt% clay loading (Fig. 3(iv)).

3-2. Pervaporation

3-2-1. Copolymer Composition, NaMMT Clay% and FeNPs %

The effect of copolymer composition and filler% on pervaporation was evaluated by a central composite design (CCD) of response surface methodology (RSM), which is more systematic than the

conventional one variable at a time (OVAT) method. The design of experiments (DOE) for different input variables--copolymer composition (x_1) and filler% (x_2) (NaMMT Clay or FeNPs) on flux (y_1) and selectivity (y_2) of NaMMT clay filled/FeNP-filled membrane--shown in Table 2. The feed concentration was kept constant at 90 wt% acetone in water. In this case the linear, interactive and quadratic effect of the two synthesis variables, namely i) copolymer composition, x_1 (3 : 1, 5 : 1, 10 : 1, 15 : 1 and 20 : 1) and ii) filler%, x_2 (Clay: 0%, 1%, 1.5% and 2% or FeNPs: 0%, 2.5%, 5%, 7.5% and 10%) on two different 'responses', i.e., flux (y_1) and water selectivity (y_2), were simultaneously studied using CCD with the regressed Eq. (21a) and (21b) for flux and selectivity, respectively,

Table 2. Design of experiment (DOE) for NaMMT clay/FeNP-filled membrane

Membrane composition	AN : EA molar ratio (x_1)	NaMMT % (x_2)/ FeNP (x_2)	Flux (kg/m^{2}h) clay/FeNP (y_1)	Water selectivity clay/FeNP (y_2)
1	5	1/2.5	0.924/0.948	117/132
2	5	2/7.5	0.905/0.937	124/142
3	15	1/2.5	0.821/0.842	146/161
4	15	2/7.5	0.803/0.828	160/176
5	3	1.5/5	0.929/0.956	102/118
6	20	1.5/5	0.759/0.789	165/178
7	10	0/0	0.857/0.876	137/153
8	10	3/10	0.822/0.859	164/170
9	10	1.5/5	0.856/0.881	157/172
10	10	1.5/5	0.856/0.881	157/172
11	10	1.5/5	0.856/0.881	157/172
12	10	1.5/5	0.856/0.881	157/172
13	10	1.5/5	0.856/0.881	157/172

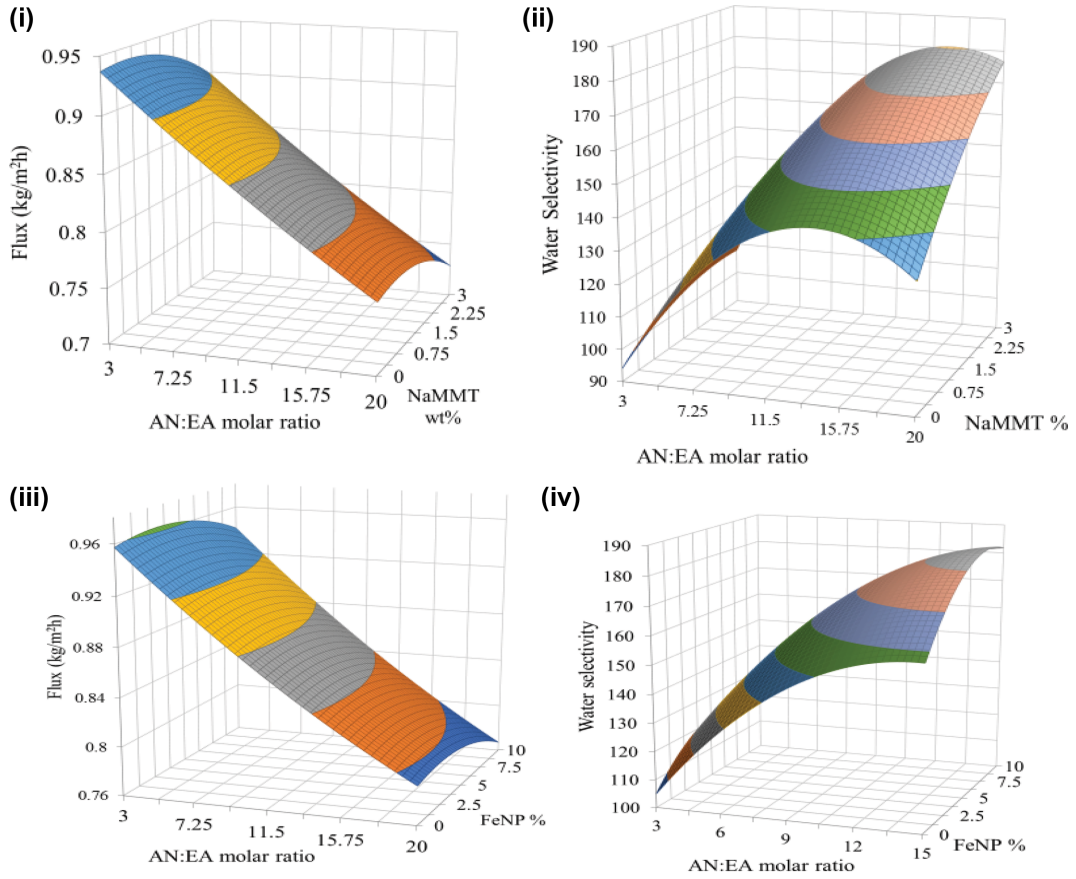


Fig. 5. Surface plot for Interactive effect of (i) and (ii) copolymer composition and clay% and (iii) and (iv) copolymer composition and iron nanoparticle% on flux and selectivity.

of NaMMT clay-filled membranes and Eq. (22a) and (22b), respectively, for FeNP-filled membranes after multiple regression. The values of the statistical parameters, adjusted R^2, F and p values, are also shown for this regression. These values also ensure good fitting to the statistical model. The interactive effect of the copolymer composition and fillers% on flux and selectivity is shown in Fig. 5(i) and (ii) for flux and selectivity, respectively, for NaMMT clay filled and unfilled membranes, while the same for FeNPs-filled and unfilled membranes are shown in Fig. 5(iii) and (iv), respectively. From the regressed Eq. (21a) and (21b) and also from Fig. 5(i) and (ii) it, is observed that with increase in AN : EA molar ratio (x_1) and NaMMT clay wt% (x_2), flux decreases as also evident from negative coefficient of linear x_1 and x_2 in Eq. (21a). Similarly, water selectivity of the membranes increases with increase in both AN : EA molar ratio and clay%. Accordingly, linear x_1 and x_2 are observed to be positive in Eq. (21b). With increase in AN : EA molar ratios (x_1), flux also decreases for FeNPs-filled membrane as shown in Fig. 5(iii), which is further confirmed by negative coefficient of x_1 in Eq. (22a). For FeNP-filled membranes a similar effect is observed for selectivity as shown in Fig. 5(iv) or Eq. (22b). The adjusted regression coefficients (R^2) for these multiple regressions were >0.94 with 'significant' 'p' values (0) for both NaMMT clay-filled and FeNPs-filled membranes. The optimization results show that the copolymer prepared with 5 : 1 molar ratio of AN : EA (noted as CP5) containing 2 wt% NaMMT clay and the CP5 membrane prepared with 5 wt% FeNPs show a flux/water selectivity of 0.903 kg/m^{2}h/125.2 and 0.937 kg/m^{2}h/140, respectively. In both cases 10% water in feed was concentrated to 93.3% and 93.9% water (90% acetone was dehydrated to 99.26% and 99.3%), respectively after pervaporation. Accordingly, the unfilled-CP5 membrane, 2 wt% NaMMT clay-filled membrane (noted as Clay2) and the 5 wt% FeNP-filled membrane (noted as FeNP5) were further subjected to sorption and pervaporation at varied feed concentrations of 75 to 99 wt% acetone in feed.

$$y_{1flux}=0.858-0.0513x_1-0.0063x_2+0.0003x_1x_2+0.0019x_1^2-0.0019x_2^2 \quad (21a)$$

Adjusted R^2=0.9929, F=561.80, Std. error 0.0043, p=0

$$y_{2sel}=153.30+21.076x_1+4.568x_2+1.625x_1x_2-9.49x_1^2-0.476x_2^2 \quad (21b)$$

Adjusted R^2=0.9103, F=40.56, Std. error 2.5, p=0

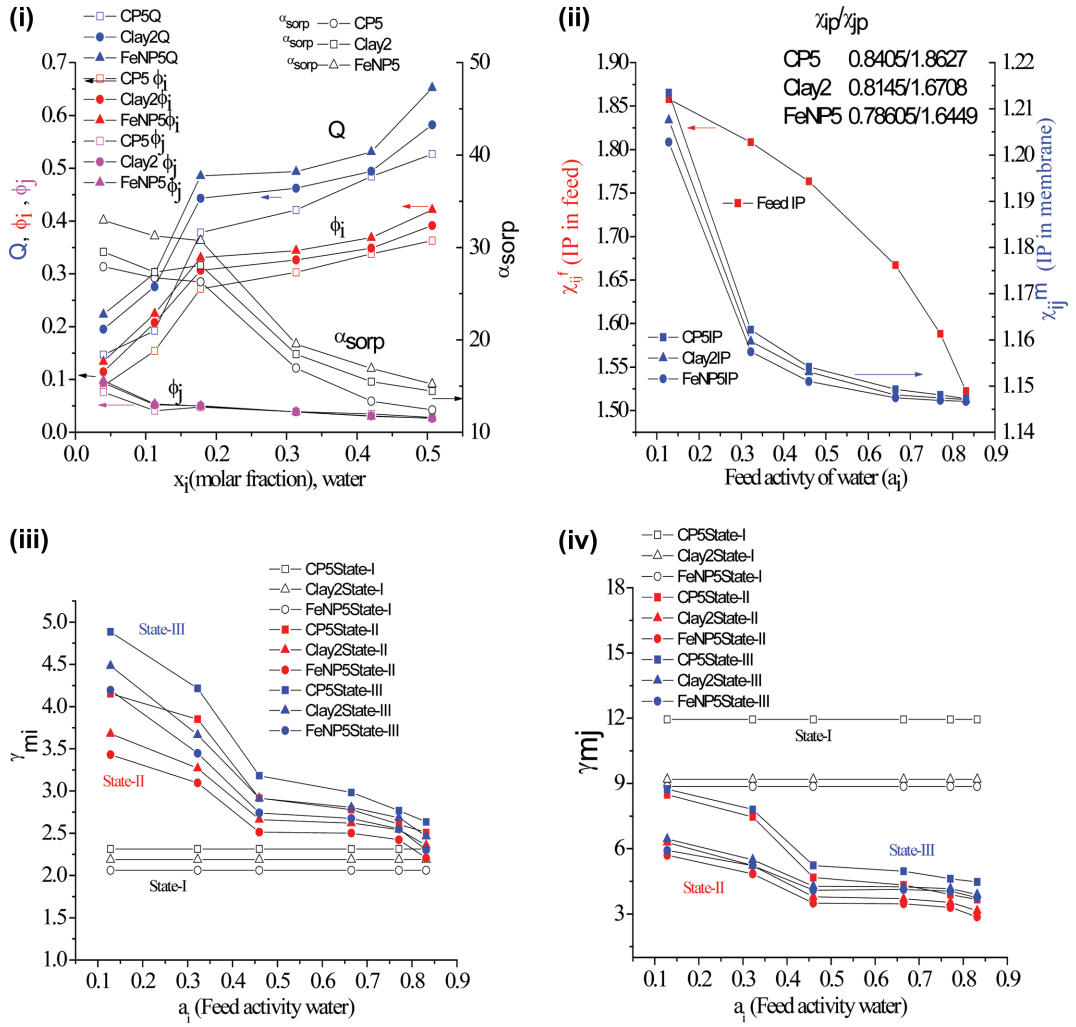


Fig. 6. Effect of (i) feed concentration on Q, ϕ_i, ϕ_j and α_{sorp}, (ii) feed activity on χ, (iii) feed activity on γ_{im} and (iv) γ_{jm} for state-1, II and III condition.

$y_{1flux}=0.879-0.0551x_1-0.0063x_2-0.0006x_1x_2+0.0005x_1^2-0.0022x_2^2$ (22a)

Adjusted $R^2=0.9569$, F=88.73, p=0, std error 0.0105

$y_{2sel}=171.40+16.986x_1+4.26x_2-1x_1x_2-12.36x_1^2-5.73x_2^2$ (22b)

Adjusted $R^2=0.9444$, F=67.98, p=0, std error 1.6

3-3. Effect of Concentration on Sorption

The effect of feed molar concentration of water (x_i) on Q, ϕ_{im}, ϕ_{jm} and α_{sorp} for CP5, Clay2 and FeNP5 membranes is shown in Fig. 6(i). It is observed that Q and ϕ_{im} increase with x_i but α_{sorp} decreases at higher feed concentration of water (x_i). On the other hand, membrane phase volume fraction of acetone (ϕ_{jm}) is much lower than water volume fraction (ϕ_{im}) at any feed concentration, indicating high water selectivity of the membranes. It is also observed that the FeNP5 membrane shows much higher Q, ϕ_{im} and α_{sorp} than the unfilled CP or NaMMT-filled Clay2 membranes over the entire feed concentration range.

3-3-1. Flory-Huggins Sorption Thermodynamics

The variation of Flory-Huggins interaction parameter (defined in supplementary 'Theory') between water and acetone in feed (χ_{ij}^f) and in membrane (χ_{ij}^m) with feed activity of water (a_i) is shown in Fig. 6(ii). It is observed that with increase in a_i, both χ_{ij}^f and χ_{ij}^m decrease, while at any a_i, $\chi_{ij}^f>\chi_{ij}^m$. In fact, the lower the value of χ, the higher will be the interaction. Thus, water-acetone interaction in the membrane is much higher than its interaction in feed, which leads to the sorption of water-acetone mixture by the membranes. As a_i increases, the interaction between water and acetone also increases because of hydrogen bonding, which also results in formation of the cluster in the feed and also in the membranes [39,56]. Thus, both χ_{ij}^f and χ_{ij}^m decrease with increase in a_i. The interaction parameter between water-membrane (χ_{ip}) and acetone-membrane (χ_{ip}) is also shown in the inset of Fig. 6(ii). It is observed that χ_{ip} is less than χ_{jp} for the three membranes and χ_{ip} for the membranes is also much lower than χ_{ij}^f or χ_{ij}^m. This explains the preferential water sorption by the hydrophilic membranes. Among the three membranes, the order of χ_{ip} is observed to be FENP5<Clay2<CP5, which also explains the order of Q, ϕ_{im} and α_{sorp} by these three membranes.

3-3-2. Solvent Coupling in Sorption Based on Flory-Huggins Thermodynamics

The coupling or mutual interaction between water and acetone (described under supplementary 'Theory') in the membrane is expressed in terms of variation of membrane phase activity coefficient of solvents (water and acetone, γ_{im} or γ_{jm}) for single component or state-I sorption, binary solvent mixture sorption without coupling or state-II sorption and state-III sorption which considers solvent coupling. From Fig. 6(iii) it is observed that for water, γ_{im} in the three states shows the following order: State-I<State-II<State-III. This positive deviation of water concentration in the membranes in coupled sorption in State-III with respect to state-I sorption in the membrane signifies the strong electrostatic interactions between the polymer membranes and water. This leads to increased sorption. The positive coupling effect of acetone on water sorption is also evident from the highest γ_{im} in the state-III condition which considers solvent coupling. It is also observed that with increase in feed water activity (a_i), solvent coupling decreases and the state-III sorption approaches state-I. In fact, at lower a_i, water-acetone interaction dominates, resulting in positive coupling effect of acetone on sorption of water. As the concentration of water in feed increases, the interaction between water and the hydrophilic membranes becomes more pronounced than the water-acetone interaction. This results in reduced coupling effect of acetone on sorption. The opposite trend is observed for acetone sorption in membrane (γ_{jm}). In this case the presence of water decreases the sorption of acetone by the membranes, i.e., for acetone state-III γ_{jm} is lower than the state-I or state-II γ_{jm} as observed in Fig. 6(iv). Similar results were also reported elsewhere, i.e., for sorption of IPA-water binary mixtures with poly(acrylonitrile-co-methylmethacrylate) membrane [57] and ethanol-water mixtures with cross-linked chitosan membranes [58], the state-III γ_{jm} of IPA and ethanol, respectively, were also reported to be less than its state-II and state-I activity coefficient.

3-3-3. Solvent Coupling in Sorption Based on ENSIC Model

The assumption of the concentration independent χ_{ip} or χ_{jp} is one of the major limitations of Flory-Huggins thermodynamics.

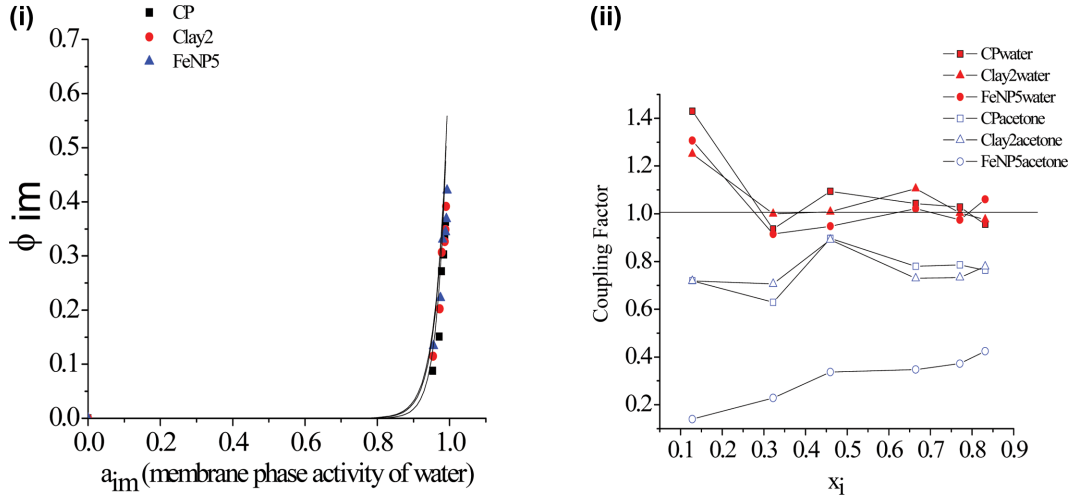


Fig. 7. (i) ENSIC fitting, (ii) effect of feed concentration on coupling factor.

This may be the reason that the order of relative sorption by the different membranes cannot be explained by this model. The ENSIC model (described under supplementary 'Theory') relates volume fraction of a polar solvent with its activity (a_i) in the membrane. The plot of the membrane phase activity and volume fraction of water as per ENSIC supplementary Eq. (13) is shown in Fig. 7(i). The experimental sorption data is observed to show a good fitting with r^2>0.95 for the membranes. The ENSIC interaction parameter between membrane and polymers, k_p and the same between solvents, i.e., k_s was also obtained by this exponential regression. Accordingly, for CP5, Clay2 and FeNP5 membranes, the k_p/k_s were found to be 0.0017/3.72, 0.0029/3.19 and 0.0091/3.07, respectively, for water and 0.209/3.21, 0.158/1.54 and 0.224/1.74, respectively for acetone. When k_p equals k_s, the sorption is of Henry's

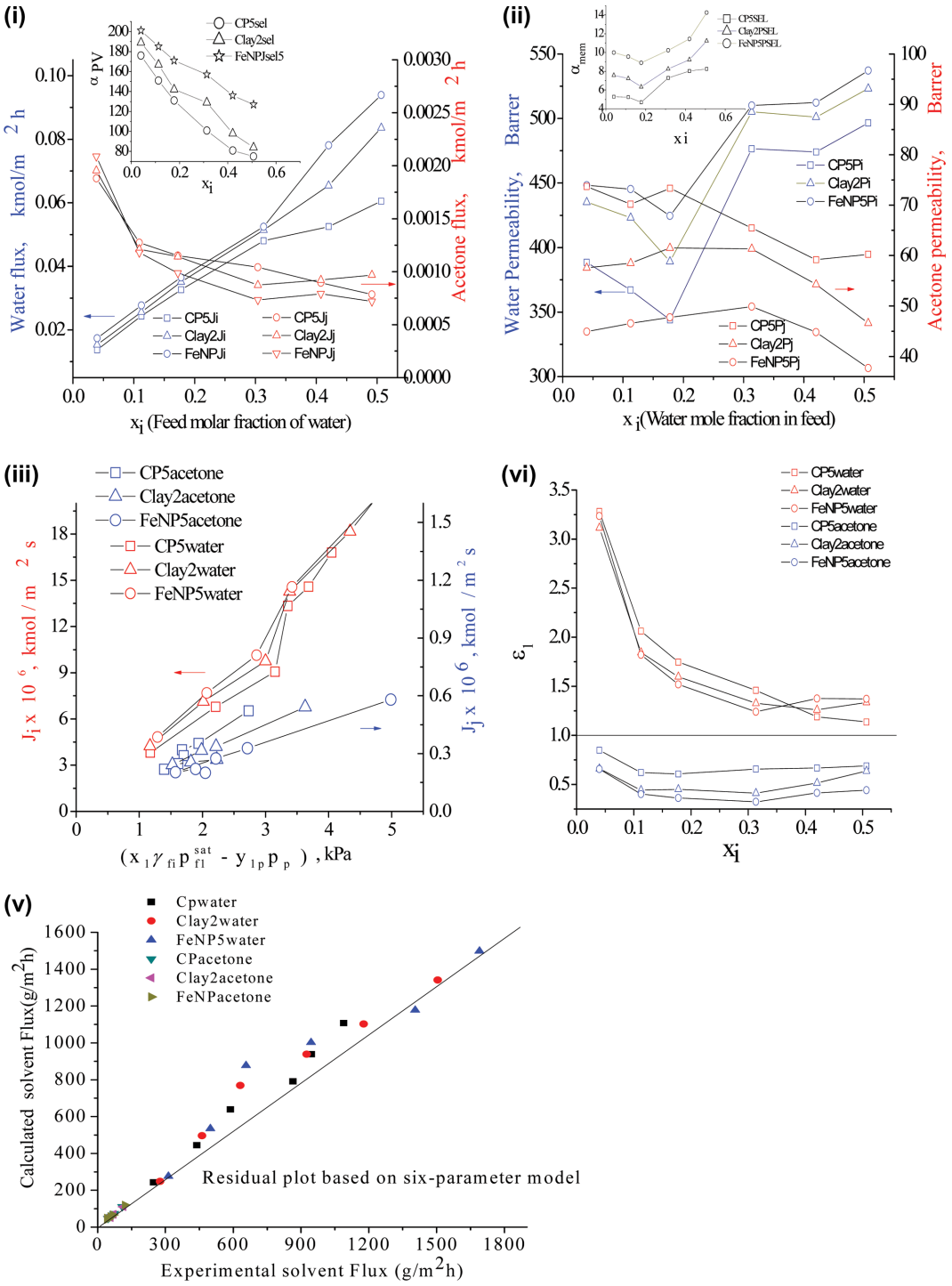


Fig. 8. Effect of feed concentration on (i) flux and (ii) permeability and intrinsic membrane selectivity (α_{mem}); (iii) flow coupling and plasticization in flux, (iv) phenomenological deviation constant (ε_i), (v) residual plot of experimental and calculated solvent flux.

type, while the higher the difference between k_s and k_p, the higher will be the solvent coupling and subsequent solvent clustering in the membranes [56]. In the present case also, the k_s values of the membranes are observed to be much higher than k_p values. The quantitative solvent coupling based on ENSIC model was obtained in terms of coupling factor (CF). CF is defined as the ratio of the experimental solvent volume fraction based on solvent 1/solvent 2/membrane ternary system to the same volume fraction (CF=$\phi_{imexpt}/\phi_{imENSIC}$) based on binary solvent 1/solvent 2 interpolated from ENSIC model supplementary Eq. (13) [59]. These are shown in Fig. 7(ii). The CF of water and acetone shows similar trend as observed for solvent coupling based on Flory-Huggins thermodynamics. Here also a positive coupling effect at low water concentration in feed is observed for water, while acetone shows negative deviation from unity signifying reduction of acetone sorption in the presence of water. Similar CF_{ENSIC} values were also reported elsewhere [59,60].

3-4. Effect of Concentration on Pervaporation

The effect of feed molar concentration of water (x_i) on partial water and acetone molar flux (J_i and J_j, respectively) and water selectivity (α_{PV}) is shown in Fig. 8(i). Similar to sorption, J_i also increases almost linearly with x_i. However, the hydrophilic membranes become plasticized at higher feed concentration (x_i>0.3) when the nanoparticle-filled membranes show very high J_i. Similarly, α_{PV} decreases exponentially with x_i. It is also observed that the membranes show much higher J_i than J_j and the variation of J_j with x_i is also marginal when x_i>0.2. The effect of x_i on partial permeability of i, j and intrinsic membrane selectivity, i.e., P_i, P_j and α_{mem}, respectively, is shown in Fig. 8(ii). It is observed that over the entire feed concentration range P_i>>P_j. The high water permeability (P_i) of these membranes may be ascribed to the strong electrostatic interaction of the hydrophilic functional groups, i.e., nitrile, acrylates and also the clay and iron nanoparticles of the membranes with water molecules as also reported for similar filled membranes [61]. This strong electrostatic interaction leads to the formation of water clusters, which also prevents movement of acetone molecules towards the membrane. Further, much lower fugacity of acetone molecules (f_j) in comparison to water also results in lower acetone permeability (P_j). It is also observed that initially P_i decreases with increase in x_i and at higher x_i (x_i>0.2-6 wt% water in feed) P_i increases, though above around 12.5 wt% water in feed (x_i>0.3) the variation of P_i with x_i is marginal. In contrast, P_j decreases over the entire feed concentration range. In fact, permeability is a thickness and vapor pressure normalized flux (Eq. (6a)). With increase in x_i, the fugacity of water (f_i) also increases, which more than offsets the increase in J_i with x_i and thus P_i decreases. However, at higher x_i, J_i increases at higher rate than f_i resulting in increase in P_i. For acetone, over the entire feed concentration range the increase in f_j offsets the increase in flux (J_j) and thus P_j decreases with x_i. Hence, the variation of permeability with concentration is ascribed to the relative change of solvent flux and fugacity with feed concentration. Since intrinsic membrane selectivity (α_{mem}) is the ratio of P_i to P_j, it also varies in a similar way, i.e., initially it decreases with x_i since P_i also follows the same trend. However, as P_i increases at higher feed concentration, α_{mem} follows the same trend.

3-4-1. Coupling and Plasticization in Flux

Combining Eq. (6a) and supplementary Eq. (20),

$$J_1=\frac{P_{o1}}{L}\exp\left(-\frac{E_{p1}}{RT}\right)(x_1\gamma_{f1}p_{f1}^{sat}-y_{1p}p_p) \tag{23}$$

The pre-exponential factor P_{o1} or membrane thickness L is constant for a specific membrane. Hence, at a fixed feed temperature the variation of partial flux of solvent 1 (i or j) with the driving force, i.e., should be linear. Any deviation from linearity signifies flow coupling and plasticization in permeation [62]. Accordingly, the deviation of water and acetone molar flux from linearity at varied ($x_i\gamma_{fi}p_{fi}^{sat}-y_{ip}p_p$) is observed in Fig. 8(iii). This deviation in linearity confirms that the flux of one component is strongly influenced by the presence of the other component through flow coupling and plasticization in the membranes [62]. The influence of the interaction between permeants and permeant-membrane interaction on permeate flux is also quantitatively expressed in terms of phenomenological deviation constant defined as [63]

$$\varepsilon_1=\frac{J_{1expt}}{J_1^{ideal}} \tag{24}$$

where J_{1expt} and J_1^{ideal} are the experimental and ideal molar flux of solvent 1, respectively. The ideal molar flux of solvent 1, J_1^{ideal}, in the binary mixture with molar concentration of $x_1$is obtained from its pure (single) component flux J_o as $J_1^{ideal}=J_ox_i$ (24a).

From Fig. 8(iv) it is observed that water shows much higher ε_i than unity, indicating strong positive coupling effect of acetone on water flux, which is more significant at low x_i when the strong interaction between the polar solvents water and acetone is higher than the interaction between the hydrophilic membranes and the small amount of water present in the feed. As the amount of water increases in feed, i.e., as x_i increases, membrane-water interaction starts dominating over water-acetone interaction and hence ε_i decreases and approaches unity at higher x_i in feed. On the other hand, an opposite trend is observed for acetone (ε_j). In this case, at very high x_j in feed (very low x_i), ε_j is close to unity. However, with increase in water concentration in feed the hydrophilic membranes preferably permeate water and thus water shows negative coupling effect on acetone. At high x_i (x_i>0.3) in feed, the acetone flux (J_j) is very low and its variation with x_i is also marginal as observed in Fig. 8(i). Accordingly, when x_i>0.3, the variation of ε_j with x_i is also not significant as observed in Fig. 8(iv).

3-4-2. Determination of D_{io} and D_{jo} by Six-parameter Model

The six parameters, the four plasticization coefficients (A_{ii}, A_{ij}, A_{jj} and A_{ji}) and D_{io} and D_{jo}, as obtained from the multiple linear regression of supplementary Eq. (18) for water (i) and supplementary Eq. (18a) for acetone (j) are shown in Table 3 for the three membranes. The regression coefficients (r^2) for these fittings are 0.94 to 0.98 as shown in Table 3, which indicates close fitting of the experimental flux data to this model. The ability of water (i) or acetone (j) for self-diffusion is evaluated in terms of self-plasticizing coefficients, i.e., the positive values of A_{ii} or A_{jj} indicate significant self-diffusion of i or j. The membranes also show positive A_{ij} values, which implies coupling effect of acetone on diffusion of water. The negative A_{ji} values indicate the negligible effect of water on diffusion of acetone. The diffusion coefficient of water at infinite dilu-

Table 3. Model parameters and diffusion coefficients of solvents at infinite dilution

Membrane	$D_{io}\times10^{10}$ m^2/s	A_{ii}	A_{ij}	Adjusted R^2	$D_{jo}\times10^{11}$ m^2/s	A_{jj}	A_{ji}	Adjusted R^2
CP	1.82	3.34	2.598	0.98306	6.8	10.569	−1.262	0.98084
Clay 2	1.87	3.342	1.304	0.93918	4	15.9496	−1.07222	0.92702
FeNP5	1.48	4.163	0.952	0.87504	5.5	12.437	−0.75226	0.9469

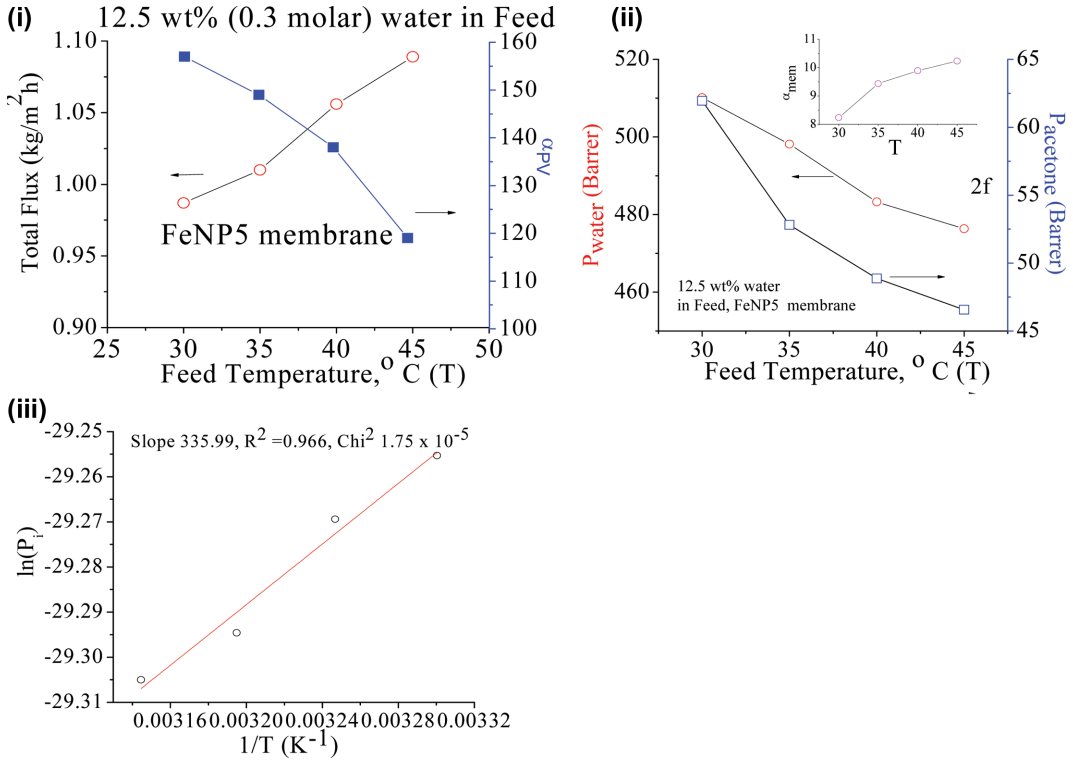


Fig. 9. Effect of temperature on (i) total flux and selectivity, (ii) permeability and membrane selectivity and (iii) Arrhenius plot with water permeability for 12.5 wt% (0.3 molar) water in feed.

tion, D_{io}, is observed to be higher than the same of acetone (D_{jo}), which may be because of smaller kinetic diameter of water (2.6 Å) than acetone (4.6 Å) [64]. Similar values of D_{io} and D_{jo} were also reported for acetone-water mixture with other membranes [10,14].

3-5. Effect of Temperature on Pervaporation

Among the three filled membranes, the filled FeNP5 membrane showing the highest flux and selectivity for water was used for flux study at 30 °C, 35 °C, 40 °C and 45 °C. This is shown in Fig. 9(i) and 9(ii) for flux and permeability, respectively. It is observed that with the increase in temperature, flux increases. This may be because permeation through the membrane is an activated process and at higher temperature vapor pressure of the solvent increases resulting in higher flux. However, at higher temperature, large amounts of acetone molecules also permeate through the membranes. This is because of increase in transient free volume in the membrane matrix. The transient-free volume of the membrane matrix increases due to increase in segmental motion of the polymer chains at higher temperature. From Fig. 9(ii) it is observed that unlike flux, solvent permeability decreases with increase in temperature, which may be ascribed to the increase in vapor pressure and fugacity with temperature. This effect more than offsets the increase in flux with temperature. The effect of temperature on intrinsic membrane selectivity (α_{mem}) is shown in the inset of the same figure. It is observed that α_{mem} also increases with temperature. The plot of ln(P_i) against inverse of absolute temperature is shown in Fig. 9(iii). The activation energy for permeation of water as obtained from the Arrhenius plot was 3.15 kJ/deg·mol. This is in good agreement with other reported activation energies for acetone-water mixtures with different polymer membranes [10,14].

3-6. Stability of the Membrane

The filled membranes (Clay1 and FeNP5) were repeatedly used for pervaporative dehydration of 90 wt% acetone for a week, which showed consistent flux and water selectivity (not shown). There was marginal change of mechanical properties of the membrane before and after use. Accordingly, the TS/EAF of clay1 and FeNP5 membrane before first use and after repeated uses for a week was found to be 30 MPa/28 mm and 27 MPa/32 mm for Clay1 and 40 MPa/15 mm and 37 MPa/18 mm for FeNP5 membrane. The FTIR analysis of the unused and used membrane shown in Fig. 10(i) for Clay1 and 10(ii) for FeNP5 membrane also ensures no change in chemical structure or leaching of clay or iron nanoparticles from the membranes after repeated use.

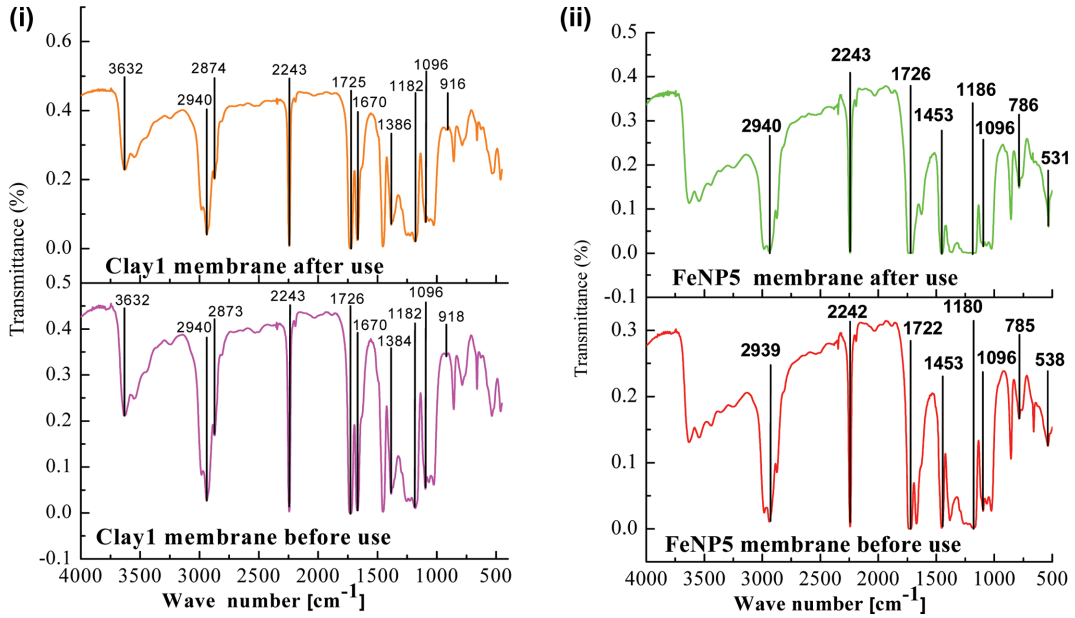


Fig. 10. FTIR of the (i) Clay1, (ii) FeNP5 filled membrane before and after pervaporation.

Table 4. Comparison of pervaporation results of the present membranes with other reported membranes for separation of acetone-water mixture

Membranes	Feed concentration of water (wt%)	Permeate flux (kg/m^2 h)	Water selectivity	References
Poly(2,6-dimethyl-1,4 phenylene oxide) (PPO) supported imide containing poly (amic acids) (PI-PAA)	10	0.22	2.4	[8]
Polyelectrolyte membrane (Symplex, GKSS)	20	4.3	100	[10]
Acrylonitrile-maleic anhydride copolymer membrane	10	0.34	5.4	[14]
Acrylonitrile with 2-hydroxyethyl methacrylate (PANHEMA-2)	2.5	0.029	16.73	[29]
Glutaraldehyde crosslinked chitosan modified with maleic anhydride	10	0.117	1791	[30]
Hydrophilic silicalite-1nanocrystal-layered membrane	10	0.108	110	[31]
PAN-b-PEG-b-PAN	5	0.274	412.8	[32]
Poly (diallyl dimethyl ammonium chloride) coated ZrO_2/ poly(sodium styrene sulfonate coated ZrO_2 on PAN support	5	1.24	361	[33]
Chitosan-PVA-carbon nano tube-PVDF 3 layers	5	0.089	1,450	[65]
P84 hollow fiber crosslinked with ethylene diamine	15	1.825	53.48	[66]
PAN-HEMAgrafted PVA	20	0.200	120	[67]
2% NaMMT filled 5 : 1 poly(AN-co-EA)	10	0.903	125.20	Present work
5% FeNP filled 5 : 1 poly(AN-co-EA)	10	0.937	140	Present work

4. Comparison with Reported Results

It is difficult to find a suitable polymer membrane for dehydration of acetone since highly concentrated acetone attacks most of the polymer membranes. The separation performance of the filled copolymer membrane, i.e. Clay2 and FeNP5 membranes, showing the optimum performance for separation of 90 wt% acetone is compared with other few membranes reported so far for pervaporative dehydration of acetone in Table 4. From the results given in Table 4 it is evident that for the same feed concentration, the present nanocomposite membranes show much higher flux and water selectivity than the other membranes reported for acetone dehydration. The iron nanoparticles were prepared in-situ within the polymer membrane from low cost ferrous and ferric salts, and thus the resulting FeNP filled membrane will be of much lower cost than the NaMMT nanoclay filled membranes. However, FeNP filled membranes show higher flux and selectivity than the clay filled membranes and also other reported FeNP-filled membranes. Among the other reported membranes, the maleic anhydride modified chitosan membrane [31] shows exceptionally high selectivity but much lower flux than the present membrane.

CONCLUSION

Several filled membranes were prepared by in-situ incorpora-

tion of nano size NaMMT and FeNP in the poly(AN-co-EA) copolymer prepared with varied molar ratio of AN and EA. The TS and EAF of the unfilled membranes increased with increase in the molar% of AN in the polymer. Below 3 : 1 molar ratio of AN and EA, the membrane polymer became too soft to be used for PV study, while above AN : EA molar ratio of 20 : 1, the membranes were very brittle and could not be used as membrane for PV. The entrapment of clay and FeNP in the copolymer membranes was confirmed with FTIR, XRD, SEM, TEM and EDAX analysis. SEM analysis suggested uniform distribution of the nano filler in the membrane without any significant agglomeration. TEM analysis showed an average 50 nm size of the synthesized FeNPs. The TEM-EDAX showed the elemental composition of the membrane. The flux of acetone-water mixture increased with increase in EA molar% in the membrane at the cost of water selectivity. Clay and FeNPs increased both flux and selectivity of the filled copolymer membranes. For the same feed concentration and temperature the FeNP filled copolymer membrane showed higher flux and selectivity than the clay filled copolymer membranes. The coupling effect of acetone on sorption and pervaporation of water decreased at higher feed water concentration when water-membrane interaction became stronger than water-acetone interaction. The permeation data showed good fitting to the six-parameter solution-diffusion model. The filled membranes also showed long-term stability and remained intact after repeated use. These chemically resistant hydrophilic membranes may also be used for dehydration of other polar solvents by pervaporation.

SUPPORTING INFORMATION

Additional information as noted in the text. This information is available via the Internet at http://www.springer.com/chemistry/journal/11814.

REFERENCES

1. G. Fytas, A. Patkowski, G. Meier and T. Dorfmuller, *Macromolecules*, **15**, 870 (1982).
2. I. C. McNeill and M. H. Mohammed, *Polym. Degrad. Stab.*, **48**, 189 (1995).
3. S. Oswal, M. H. Patel and S. G. Patel, *Int. J. Polym. Matter Po.,* **56**, 307 (2007).
4. J. Machotov, L. Zárybnick, R. Bačovsk and E. Černošková, *Polym. Plast. Technol. Eng.*, **55**, 423 (2015).
5. A. S. Singha and R. K. Rana, *Carbohydr. Polym.*, **87**, 500 (2012).
6. F. Q. Nie, Z. K. Xu, X. J. Huang, P. Ye and J. Wu, *Langmuir*, **19**, 9889 *(*2003).
7. S. Choudhury and S. K. Ray, *Sep. Purif. Technol.*, **179**, 335 (2017).
8. M. Olukman and O. Şanl, *Chem. Eng. Process.*, **98**, 60 (2015).
9. P. Das and S. K. Ray, *J. Membr. Sci.*, **507**, 81 (2016).
10. S. Ray and S. K. Ray, *Sep. Sci. Technol.*, **40**, 1583 (2005).
11. S. Choudhury and S. K. Ray, *Ind. Eng. Chem. Res.*, **58**, 4581 (2019).
12. H. S. Samanta, S. K. Ray, P. Das and N. R. Singha, *J. Chem. Technol. Biot.*, **87**, 608 (2012).
13. H. S. Samanta and S. K. Ray, *Sep. Purif. Technol.*, **146**, 176 (2015).
14. S. Ray and S. K. Ray, *J. Membr. Sci.*, **270**, 73 (2006).
15. M. S. Jyothi, *J. Environ. Manage.*, **242**, 415 (2019).
16. P. D. Suhas, R. V. Anjanapura, J. M. Han and T. M. Aminabhavi, *RSC Adv.*, **3**(38), 17120 (2013).
17. S. P. Dharupaneedi, R. V. Anjanapura, J. M. Han and T. M. Aminabhavi, *Ind. Eng. Chem. Res.*, **53**(37), 14474 (2014).
18. P. D. Suhas, T. M. Aminabhavi, J. M. Han and A. V. Raghu, *RSC Adv.*, **5**(122), 100984 (2015).
19. S. H. Chen, R. M. Lioua, C. L. Lai, M. Y. Hunga, M. H. Tsaib and S. L. Huang, *Desalination*, **234**, 221 (2008).
20. H. G. Premakshi, A. M. Sajjan, A. A. Kittur and M. Y. Kariduraganavar, *J. Appl. Polym. Sci.*, **41248**, 1 (2015).
21. A. Selim, N. Valentínyi, T. Nagy, A. J. Toth, D. Fozer, E. Haaz and P. Mizsey, *Chin. J. Chem. Eng.*, **27**, 1595 (2019).
22. S. Chaudhari, Y. S. Kwon, M. J. Moon, M. Y. Shon, S. E. Nam and Y. Park, *Bull. Korean Chem. Soc.*, **11008**, 1 (2016).
23. M. K. Mandal, S. B. Sant and P. K. Bhattacharyaa, *Colloids Surf. A: Physicochem. Eng. Asp.*, **373**, 11 (2011).
24. M. Sairam, B. V. K. Naidu, S. K. Nataraj, B. Sreedhar and T. M. Aminabhavi, *J. Membr. Sci.*, **283**, 65 (2006).
25. M.Olukman, O. Sanlı and E. K. Solak, *Vacuum*, **120**, 107 (2015).
26. G. Dudek, M. Gnus, R. Turczyn, A. Strzelewicz and M. Krasowska, *Sep. Purif. Technol.*, **133**, 8 (2014).
27. C. Zhao, Z. Jiang, J. Zhao, K. Cao, Q. Zhang and F. Pan, *Ind. Eng. Chem. Res.*, **53**, 1606 (2014).
28. M. Uno, A. Nakae, J. Sudoh, Y. Hirose and M. Hirata, *J. Chem. Eng. Japan*, **4**, 33 (1971).
29. Q. Yeang, S. Zein, A. Sulong and S. Tan, *Sep. Purif. Technol.*, **107**, 252 (2013).
30. D. Mangindaan, G. Shi and T. Chung, *J. Membr. Sci.*, **458**, 76 (2014).
31. W. Zhang, G. Li, Y. Fang and X. Wang, *J. Membr. Sci.*, **295**, 130 (2007).
32. Q. Zhao, J. Qian, Q. An, Z. Zhu, P. Zhang and Y. Bai, *J. Membr. Sci.*, **311**, 284 (2008).
33. J. Li, G. Zhang, J. Shulan, N. Wang and A. Wei, *J. Membr. Sci.*, **415**, 745 (2012).
35. M. Hirata, S. Ohe and K. Nagahama, *Computer aided data book of vapor-liquid equilibria*, Kodansha Limited, Elsevier Scientific Co. Tokyo (1985).
36. M. H. V. Mulder and C. A. Smolders, *J. Membr. Sci.*, **17**, 289 (1984).
37. M. Hana, B. Zhao, X. M. Zhang and W. J. Zhang, *Chem. Eng. Process*, **47**, 245 (2008).
38. R. Guo, C. Hu, B. Li and Z. Jiang, *J. Membr. Sci.*, **289**, 191 (2007).
39. E. Favre, Q. T. Nguyen, R. Clement and J. Nrel, *J. Membr. Sci.*, **117**, 227 (1996).
40. P. Shao and R. Y. M. Huang, *J. Membr. Sci.*, **287**, 162 (2007).
41. S. B. Kuila and S. K. Ray, *Sep. Purif. Technol.*, **89**, 39 (2012).
42. M. Villegasa, E. F. C. Vidaurrea, A. C. Habertb and J. C. Gottifredi, *J. Membr. Sci.*, **367**, 103 (2011).
43. D. Y. Godovsky, A. V. Varfolomeev, G. D. Efremova, V. M. Cherepanov, G. A. Kapustin, A. V. Volkov and M. A. Moskvina, *Adv. Mater. Opt. Electron.*, **9**, 87 (1999).
44. M. A. Hoque, M. R. Ahmed, G. T. Rahman, M. T. Rahman, M. A. Islam, M. A. Khan and M. K. Hossain, *Results Phys.*, **10**, 434 (2018).
45. K. Katsuraya, K. Hatanaka, K. Matsuzaki and M. Minagawa, *Polymer*, **42**, 6323 (2001).
46. Y. Wang, L. Xu, M. Wang, W. Pang and X. Ge, *Macromolecules*, **47**,

3901 (2014).
47. A. S. Brar, Sunita, *Eur. Polym. J.*, **28**(7), 803 (1992).
48. X. Liu, Y. Makita, Y. L. Hong and Y. Nishiyama, *Macromolecules*, **50**, 244 (2017).
49. M. Kurata and Y. Tsunashima, in *Polymer handbook*, 4th Ed., J. Brandrup, E. H. Immergut and E. A. Grulle Eds., Wiley (2003).
50. A. Ju, Y. Yan, D. Wang, J. Luo, M. Ge and M. Li, *RSC Adv.*, **4**, 64043 (2014).
51. N. Chatterjee, S. Basu, S. K. Palit and M. M. Maiti, *J. Polym. Sci., Part B: Polym. Phys.*, **33**, 1705 (1995).
52. R. Zahedsheijani, M. Faezipour, A. Tarmian, M. Layeghi and H. Yousefi, *Eur. J. Wood Prod.*, **70**, 565 (2012).
53. J. Quan, Y. Yu, W. C. Branford, G. R. Williams, D. G. Yu, W. Nei and L. M. Zhu, *Colloids Surf. B*, **88**, 304 (2011).
54. A. Lassoued, M. S. Lassoued, B. Dkhil, S. Ammar and A. Gadri, *J. Mater. Sci. Mater.*, **29**, 8142 (2018).
55. S. M. Pawde and K. Deshmukh, *J. Appl. Polym. Sci.*, **110**, 2569 (2008).
56. M. Modesti, C. Dall'Acqua, A. Lorenzetti and E. Florian, *J. Membr. Sci.*, **229**, 211 (2004).
57. S. B. Kuila and S. K. Ray, *Chem. Eng. Res. Des.*, **91**, 377 (2013).
58. J. Ren and C. Jiang, *J. Membr. Sci.*, **140**, 221 (1998).
59. A. Jonquières, L. Perrin, S. Arnold, R. Clément and P. Lochon, *J. Membr. Sci.*, **174**, 255 (2000).
60. E. Drioli, S. Zhan and A. Basile, *J. Membr. Sci.*, **81**, 43 (1993).
61. D. P. Suhas, T. M. Aminabhavi and A. V. Raghu, *Appl. Clay Sci.*, **101**, 419 (2014).
62. W. R. Berendsen, P. Radmer and M. Reuss, *J. Membr. Sci.*, **280**, 684 (2006).
63. S. Marx, P. V. Gryp, H. Neomagus, R. Everson and K. Keizer, *J. Membr. Sci.*, **209**, 353 (2002).
64. H. S. Samanta and S. K. Ray, *Sep. Purif. Technol.*, **143**, 52 (2015).
65. G. A. Polotskaya, Y. P. Kuznetsov, M. Y. Goikhman, I. V. Podeshvo, T. A. Maricheva and V. V. Kudryavtsev, *J. Appl. Polym. Sci.*, **89**, 2361 (2003).
66. T. Tago, Y. Nakasaka, A. Kayoda and T. Masuda, *Micropor. Mesopor. Mater.*, **115**, 176 (2008).
67. A. Urtiaga, C. Casado, C. Aragoza and I. Ortiz, *Sep. Sci. Technol.*, **38**, 3473 (2003).

Supporting Information

Sorption thermodynamics and coupling effect for pervaporative dehydration of acetone through nanoclay and iron nanoparticle-filled copolymer membranes

Swastika Choudhury and Samit Kumar Ray†

Department of Polymer Science and Technology, University of Calcutta, 92, A. P. C. Road, Kolkata-700009
(*Received 5 May 2021 • Revised 6 July 2021 • Accepted 13 July 2021*)

THEORY

1. Interaction Parameter of Component *i* and *j*, in Feed (χ_{ij}^{f}) and membrane (χ_{ij}^{m}) based on Flory-Huggins Thermodynamics

The Flory-Huggins thermodynamic interaction parameter between solvent i (water) and j (acetone) in feed (χ_{ij}^{f}) is obtained as [36]

$$\chi_{ij}^{f}=\frac{1}{x_i\phi_j}\left[x_i\ln\left(\frac{x_i}{\phi_i}\right)+x_j\ln\left(\frac{x_j}{\phi_j}\right)+\frac{\Delta G^{E}}{RT}\right] \tag{7}$$

Where the excess free energy, ΔG^{E} is obtained as

$$\Delta G^{E}=RT(x_i\ln\gamma_{if}+x_j\ln\gamma_{jf}) \tag{7a}$$

Here ϕ_i and ϕ_j are the volume fraction of solvent i and j, respectively in binary i+j feed mixtures such that

$$\phi_i=\frac{v_i}{v_i+v_j} \tag{7b}$$

$$\phi_j=\frac{v_j}{v_i+v_j} \tag{7c}$$

Here v_i and v_j are solvent volume of i and j, respectively in feed. For obtaining interaction parameter between i and j in the membrane (χ_{ij}^{m}), χ_{ij}^{f} as obtained by Eq. (7) is plotted against ϕ_i to obtain a polynomial Eq. (8) [37]

$$\chi_{ij}^{f}=a+b\phi_i+c\phi_i^{2}+d\phi_i^{3} \tag{8}$$

The values of a, b, c and d as obtained by the polynomial regression with regression coefficient, $r^2=1$ were 1.884, −2.6662, 5.857 and −7.648, respectively.

Under similar condition the χ_{ij}^{m} is also obtained from the following regressed Eq. (8a)

$$\chi_{ij}^{m}=a+bu_i+cu_i^{2}+du_i^{3} \tag{8a}$$

Where u_i is relative volume fraction of component *i* in membrane such that

$$u_i=\frac{\phi_{im}}{\phi_{im}+\phi_{jm}} \tag{8b}$$

1-1. Interaction Parameter between Solvents and Membrane Polymer

Based on Flory-Huggins theory the effect of viscoelasticity on chemical potential can be ignored. Accordingly, the χ_{im} and χ_{jm} are obtained from the pure component 1 (1 is i or j) sorption as [36]

$$\chi_{1p}=\frac{-\ln(1-\phi_p)-\phi_p}{\phi_p^{2}} \tag{9}$$

Where the polymer volume fraction, ϕ_p in solvent-membrane binary system is obtained from the wt. of the swollen membrane (m_s), dry membrane (m_d), solvent and membrane-polymer density (ρ_1 and ρ_p, respectively), as

$$\phi_p=\left(1+\frac{m_s\rho_p}{m_d\rho_1}\right)^{-1} \tag{9a}$$

1-2. Membrane Phase Activity Coefficient and Solvent Coupling

For polymer-solvent binary system, the activity of single solvent 1 in the membrane is

$$a_{1m}=x_{1m}\,\gamma_{1m} \tag{10}$$

However, the solvent mole fraction is difficult to measure because molecular weight of membrane polymer is much higher than molecular weight of the solvent. Further, polymer has a molecular weight distribution instead of a single molecular weight. Thus, the solvent mole fraction term is replaced with solvent volume fraction. Further, for pure component sorption, $a_{1m}=1$. Accordingly, the *State-I* activity coefficient of single solvent 1 (i or j) is expressed as [36]

$$\gamma_{1m}=\frac{a_{1m}}{\phi_{1m}}=\frac{1}{\phi_{1m}} \tag{10a}$$

Similarly, *State-II* activity coefficient for binary solvent mixtures in membrane without considering coupling effect is obtained as [38]

$$\ln\gamma_{1m}=\phi_p+\chi_{ip}\phi_p^{2}=(1-\phi_{1m})+\chi_{ip}(1-\phi_{1m})^{2} \tag{11}$$

The state-III activity coefficient including solvent coupling for solvent i and j is obtained as [38]

$$\ln\gamma_{im}=\phi_p+\chi_{ip}\phi_p^{2}+\left(1-\frac{V_i}{V_j}\right)\phi_j+\chi_{ij}^{m}\phi_j^{2}+\left(\chi_{ij}^{m}+\chi_{ip}-\frac{V_i}{V_j}\chi_{jp}\right)\phi_j\phi_p-u_iu_j\phi_j\frac{\partial\chi_{ij}^{m}}{\partial u_2} \tag{12a}$$

$$\ln\gamma_{jm}=\phi_p+\chi_{ip}\phi_p^{2}+\left(1-\frac{V_j}{V_i}\right)\phi_i+\frac{V_j}{V_i}\chi_{ij}\varphi_i^{2}+\frac{V_j}{V_i}\left(\chi_{ij}^{m}+\chi_{ip}+\frac{V_i}{V_j}\chi_{jp}\right)\phi_i\phi_p+\frac{V_j}{V_i}u_i^{2}\phi_j\frac{\partial\chi_{ij}^{m}}{\partial u_2} \tag{12b}$$

2. Solvent Coupling Based on Engaged Species Induced Clustering (ENSIC) Model

The clustering of polar solvent pair water-acetone in membrane is more accurately obtained by ENSIC model Eq. (13). The ENSIC solvent-solvent interaction parameter, k_s and solvent-polymer parameter k_p is obtained by fitting the activity data and corresponding membrane phase volume fraction of the solvent in Eq. (13) [39]

$$\phi_1 = \frac{\exp(k_s - k_p)a_1 - 1}{(k_s - k_p)/k_p} \tag{13}$$

3. Diffusion Coefficient

Based on six-parameter model [40], the diffusion coefficient of solvent i and j in a solvent-i/solvent-j/membrane polymer ternary system is obtained as

$$D_i = D_{io}\exp(A_{ii}\phi_{im} + A_{ij}\phi_{jm}) \tag{14a}$$

Among the six model parameters, D_{io}, and D_{jo} are diffusion coefficient of i and j at infinite dilution, respectively, A_{ii} and A_{jj} are self-plasticization coefficient of i and j, respectively and A_{ij} and A_{ji} are coupling coefficient of j and i, respectively, i.e., A_{ij} means ability of acetone (j) to increase the diffusion of water (i) and vice versa for A_{ji}. Accordingly, the transport equation for solvent i and j will be [40,41]

$$J_i = D_{io}\exp(A_{ii}\phi_{im} + A_{ij}\phi_{jm})\frac{d\phi_{im}}{dl} \tag{15a}$$

$$\text{and } J_j = D_{jo}\exp(A_{jj}\phi_{jm} + A_{ji}\phi_{im})\frac{d\phi_{jm}}{dl} \tag{15b}$$

After integration with boundary condition at l=0, $\phi_{1m}=\phi_{1mu}$ and $\phi_{1m}=\phi_{1md}$ at l=L (where ϕ_{1mu} and ϕ_{1md} are upstream and downstream side concentration of solvent 1 in membrane, respectively), ignoring very low concentration of the permeants on the downstream (d) side of the membrane, i.e., ϕ_{imd} and ϕ_{jmd}~0

$$J_i = \frac{D_{io}\rho_m}{LA_{ii}}\{\exp(A_{ii}\phi_{imu} + A_{ij}\phi_{jmu}) - \exp(A_{ij})\} \tag{16}$$

$$J_j = \frac{D_{jo}\rho_m}{LA_{jj}}\{\exp(A_{jj}\phi_{jmu} + A_{ji}\phi_{imu}) - \exp(A_{ji})\} \tag{16a}$$

As self-diffusion is much higher than coupled diffusion, i.e., A_{ii}>> A_{ij} and A_{jj}>>A_{ji} [23]

$$J_i = \frac{D_{io}\rho_m}{LA_{ii}}\{\exp(A_{ii}\phi_{imu} + A_{ij}\phi_{jmu}) - 1\} \tag{17}$$

$$J_j = \frac{D_{jo}\rho_m}{LA_{jj}}\{\exp(A_{jj}\phi_{jmu} + A_{ji}\phi_{imu}) - 1\} \tag{17a}$$

Ignoring the very low value of $\frac{D_{1o}\rho_m}{LA_{11}}$ in comparison to flux and taking logarithm on both side

$$\ln(J_i) = \ln\left(\frac{D_{io}\rho_m}{LA_{ii}}\right) + A_{ii}\phi_{imu} + A_{ij}\phi_{jmu} \tag{18}$$

$$\ln(J_j) = \ln\left(\frac{D_{jo}\rho_m}{LA_{jj}}\right) + A_{jj}\phi_{jmu} + A_{ji}\phi_{imu} \tag{18a}$$

The multiple linear regression of $\ln J_i$ or $\ln J_j$ against feed volume fraction of i and j gives the values of the A_{ii}, A_{ij}, A_{jj} and A_{ji} from the coefficients of the membrane phase volume fractions. Similarly, the diffusion coefficients at infinite dilutions, i.e., D_{io} and D_{jo} were obtained from the intercepts of these multiple linear regression.

4. Determination of Activation Energy for Permeation

The effect of temperature on flux or permeability may be evaluated in terms of activation energy using an Arrhenius type equation. Activation energy for permeation calculated from flux data at different temperatures is not accurate since it does not include heat of vaporization. Instead solvent permeability at different temperatures gives actual activation energy [42] from the following Arrhenius type Eq. (19) and (20).

$$P_i = P_{0,i}\exp\left(-\frac{E_{pi}}{RT}\right) \tag{19}$$

$$\text{Or, } \ln P_i = P_{0,i} - \frac{E_{pi}}{RT} \tag{20}$$

Linear plotting of $\ln P_i$ against 1/T gives the value of activation energy for permeation of i (water) (E_{pi}) and pre-exponential factor (P_{0i}) from the slope and intercept, respectively.